The Imperial Crown of the Holy Roman Empire, Part I: Photoluminescence and Raman Spectroscopic Study of the Gemstones

Lutz Nasdala, Teresa Lamers, H. Albert Gilg, Chutimun Chanmuang N., Martina Griesser, Franz Kirchweger, Annalena Erlacher, Miriam Böhmler and Gerald Giester

ABSTRACT: The Imperial Crown of the Holy Roman Empire is not only a unique and outstanding symbol of European history, it is also one of the most significant works of Western goldsmiths' art from the High Middle Ages. However, little is known about the gem materials it contains. As part of an interdisciplinary research project led by the Kunsthistorisches Museum Vienna in Austria, the 172 gemstones in the crown were all conclusively identified for the first time using (non-destructive) photoluminescence and Raman spectroscopy. They include 71 blue sapphires, 50 garnets (22 almandines, 22 pyrope-almandines, five pyropes and one grossular), 20 emeralds, 13 amethysts, four chalcedonies and three spinels. In addition, 11 glass imitations of various colours were identified. Raman spectral details and inclusions in the garnets support their assignment to garnet types previously found to be used in antique and early medieval jewellery. The large red spinel in the centre of the crown's front plate is presumably part of the original crown and, thus, is one of the earliest-known spinels in a historic object, yet it yielded spectroscopic evidence of having been heated.

The Journal of Gemmology, **38**(5), 2023, pp. 448–473, https://doi.org/10.15506/JoG.2023.38.5.448

From medieval times until 1792, the Imperial Crown (see Figure 1 and the cover of this issue) was used for the coronations of kings and emperors of the Holy Roman Empire. It is octagonal, with eight gold plates (heights between 11.9 and 14.9 cm) joined together by hinges to form the circlet. Affixed to the top of the crown is a removable single arch and cross that were added later (Fillitz 1953). A removable velvet biretta was added much later, and subsequently two iron bands were riveted to the inside walls of the circlet to stabilise its form.

The circlet includes four smaller picture plates with enamelled images (figurative representations from the Bible) surrounded by blue gems and pearls, and four larger plates adorned by gemstones and pearls only. All the large stones in these eight plates are set atop openings in the gold sheet, facilitating transmitted-light illumination to brighten their colouration and overall appearance (Figure 2). In contrast, the settings in the arch and cross do not have such openings due to their double-sided construction.

The Imperial Crown contains a total of 172 gemstones in different kinds of settings on the circlet, arch and cross. These stones are mostly polished pebbles of oval to irregular shape, but some are distinctly shaped crystal fragments (i.e. green stones, identified as emeralds). A few gems with faceted shapes are considered to be later replacements.

Figure 1: The Imperial Crown of the Holy Roman Empire is shown here in a view towards the front right ('Maiestas') plate. The crown weighs 3,465 g, is 24.4 cm high and has a maximum diameter of 28.6 cm. Photo © KHM-Museumsverband (Christian Mendez); reproduced with permission.

The arrangement of the colourful stones together with 241 pearls (plus several hundred small pearls forming the letters on the arch) follows a complex concept that has already been studied in the context of medieval symbolism (Decker-Hauff 1955; Fillitz 1956). There are still many questions, however, concerning the nature of the stones themselves and their history with regard to the crown. Many adjustments, incidents of damage and repairs took place in the crown's long and eventful history, including some gem replacements (e.g. Figure 3). These are suspected in cases where the shape of the opening of the setting does not properly match the shape of the respective gemstone. On the other hand, the characteristics of some gemstones (such as old drill holes, special cuts or intaglios) indicate an ancient provenance and reuse on the crown.

Apart from a few determinations of the large stones based on visual inspection, the gemstones in the Imperial Crown have never been studied and analysed completely. An article in the Austrian newspaper *Presse* (issued 19 June 1967) titled 'Edelsteintests in der Wiener Schatzkammer' (Gem tests in the Vienna Treasury) summarised an interview with Prof. Dr Hubert Scholler, at that time director of the Mineralogical and Petrological Department of the Natural History Museum Vienna, in which he mentioned future plans to study the gems in the Imperial Crown and other historic objects in the Kunsthistorisches Museum Vienna. However, it took ten

Figure 2: Illumination from the inside of the Imperial Crown's circlet (after removal of the arch and velvet biretta) reveals that its large stones are set atop openings in their gold plates. Thus, transmitted light makes the gems appear brighter. Photo © KHM-Museumsverband (Christian Mendez); reproduced with permission.

years until gem-related assessments of the crown were made by Prof. Dr Gero Kurat, Scholler's successor as director of the department. A sketch summarising his determinations of the large stones in the cross, front plate and nape plate is shown in Figure 4. This sketch was made by Dr Rudolf Distelberger, at that time curator of the Secular & Ecclesiastical Treasury (today the Imperial Treasury Vienna). The drawing notes a date of December 1977, but it is not known whether the examination, the sketch or both were made at that time. In the archive of the Kunsthistorisches Museum Vienna, there also exists a copy of a letter dated 20 December 1977 in which a former director of the department, Dr Manfred Leithe-Jasper, thanks Prof. Kurat, together with Dr Gerhard Niedermayr, for inspecting gemstones in the treasury.

There are a number of scientific studies of gemstones in regalia from the Late Middle Ages (1300–1500 CE), such as the crowns of Saint Wenceslaus (Hyršl & Neumanova 1999) and Blanche of Lancaster (Schmetzer & Gilg 2020), but similar studies are scarce for regalia from the (earlier) High Middle Ages (1000–1300 CE; Bruni *et al.* 2021), such as the Imperial Crown described here. In 2022, a three-year interdisciplinary project 'Crown' (www.projekt-reichskrone.at) started at the Kunsthistorisches Museum Vienna. This project targets, at an advanced level, issues regarding the Imperial Crown's materials, manufacturing technology and state of preservation. It includes the application of numerous optical and analytical investigation methods, together with art-historical and historical studies such as the reassessment of written and pictorial sources, and evaluation of the crown's inscriptions. The project includes, among others, two analysis campaigns (April–July 2022 and several months in 2023). Note that conducting all the desired analyses in one extended campaign was impractical, as the removal of the crown—which is a key exhibit and tourist attraction—from its display needs to be strictly limited in time. The first campaign focused on the optical investigations of all parts of the crown with three-dimensional (3D) microscopic imaging and spectroscopic study of its gemstones, with the latter results reported here. The second campaign will comprise chemical analyses by X-ray fluorescence spectroscopy (micro-XRF and XRF mapping) of the enamel, pearls (with the aim of distinguishing freshwater vs saltwater origin) and selected gemstones.

HISTORICAL BACKGROUND

The Imperial Crown and its history have been studied many times during the last 200 years, but essential questions are still open and under debate, including

Figure 3: This view from above the circlet's front plate (after removal of the adjoining cross) shows that the central large, perforated sapphire (stone A4; width about 2.6 cm) is most likely a later replacement that does not fit well in the cramped setting and is affixed with wire. Photo © KHM-Museumsverband (Herbert Reitschuler); reproduced with permission.

the time and place of its manufacture. For a long time, it was agreed that the circlet of eight golden plates was made before 980 CE, probably for the coronation of Otto I ('the Great') in 962 CE (Decker-Hauff 1955; Kugler 1986; Wolf 1995; Staats 2006). The front cross and the arch were accepted to be later additions from the first half of the eleventh century (Fillitz 1953). Since the 1990s, this dating has been questioned by archaeologists, who link the Imperial Crown's manufacture to the time of the Salian Conrad II (Schulze-Dörrlamm 1991), who ruled the Holy Roman Empire from 1024 to 1039. Historians have even argued that the crown should be assigned to the 1138–1152 reign of Conrad III (Schaller 1997). Proposals concerning its place of manufacture include the towns of Cologne and Essen in the lower Rhine area, the Benedictine Abbey on the island of Reichenau in Lake Constance, and even goldsmiths' workshops outside present-day Germany, such as in Sicily, Lombardy or even Byzantium.

Medieval texts repeatedly mention the 'Orphan Stone' (from Latin *orphanus*), also referred to as *Pupilla* or *die Waise* (in Middle High German; often modified to *der Weise* in recent publications), as a one-of-a-kind specimen that was part of the Imperial Crown. It was perhaps the most famous gemstone of the Middle Ages in Germany (for a summary, see Buettner 2022 and Quenstedt 2022), heralded as the *aller fürsten leitesterne* ('guiding star to all princes') around 1200. The Orphan Stone was described as a pale reddish to vivid red ('carbuncle') gem that gleamed at night, mounted either

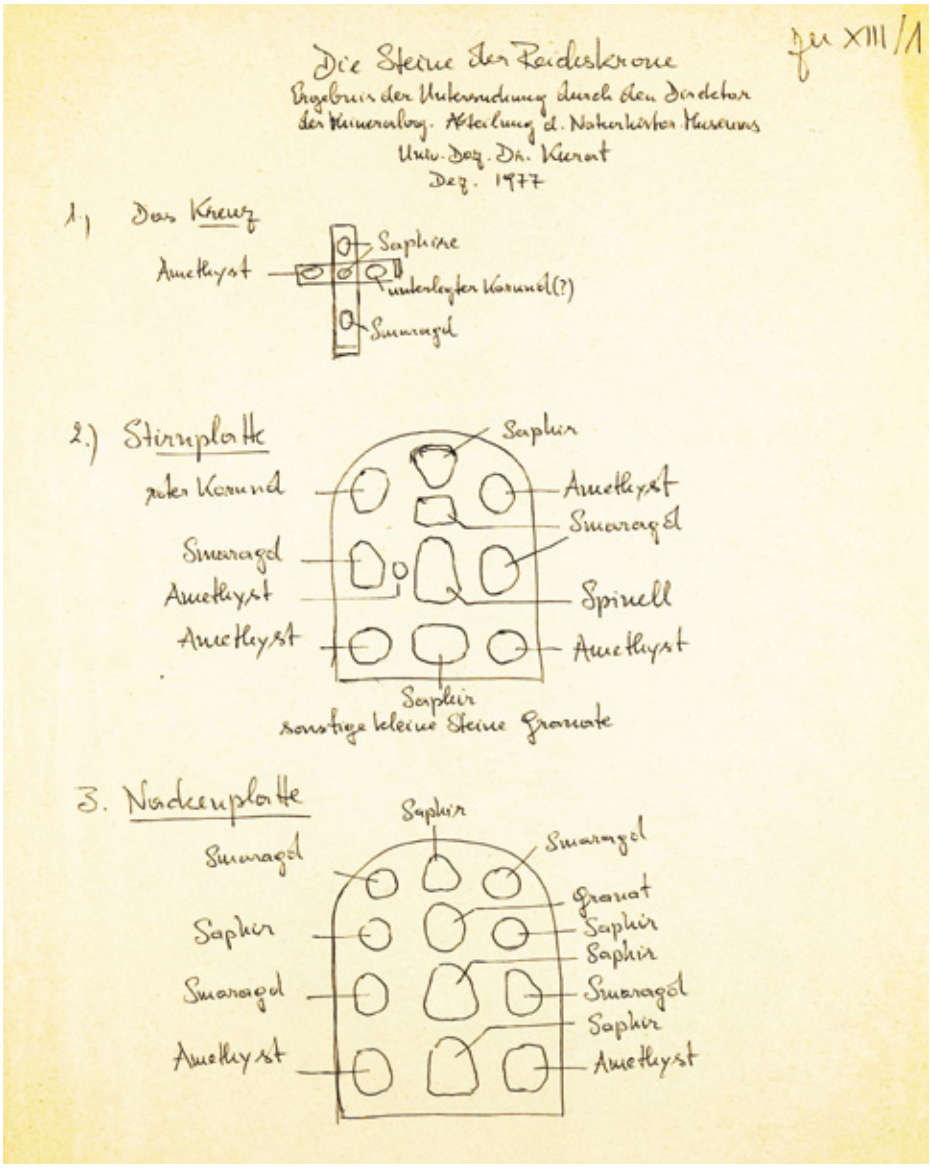

Figure 4: This sketch of the cross, front plate and nape plate notes the following (translated from German): 'The stones of the Imperial Crown. Result of the examination by the director of the Mineralogical Department of the Natural History Museum, University Lecturer Dr Kurat Dec. 1977.' All of these identifications were confirmed by the present study except for the right stone in the cross and the upper-left gem in the front plate (indicated in the sketch as *Korund*). © KHM-Museumsverband; reproduced with permission.

Figure 5: Detail from a circa 1600 copy of a 1511–13 painting by Albrecht Dürer (1471–1528) shows Charlemagne wearing the Imperial Crown of the Holy Roman Empire. The painting is anachronistic because the Imperial Crown was created at least one-and-a-half centuries after Charlemagne's reign (768–814). © KHM-Museumsverband, Picture Gallery, inv. no. 2771; reproduced with permission.

in the front plate or in the centre of the nape plate. All of these descriptions regarding the Orphan Stone were challenged recently, however, when medieval texts cited as references were declared to be purely fictional stories (Mentzel-Reuters 2004).

The Imperial Crown has had a long—and at times—eventful history. Its earlier times, especially, are rather poorly documented. Some information on its status in later times can be extracted from sixteenth- to eighteenth-century paintings and drawings (see, e.g., Figures 5 and 6). The crown was kept in many different places over the years (Kugler 1986). After 1424, it was deposited in the chapel of Heilig-Geist-Spital in Nuremberg, Germany, and only taken out for coronations, which were initially held in Aachen and later in Frankfurt am Main. Since 1800, the Imperial Crown has been kept in Vienna, except for 1938–1946 when it was brought to Nuremberg to be stored later on during World War II in the Historischer Kunstbunker (a tunnel complex under Nuremberg Castle). Since 1954, the Imperial Regalia—including the Imperial Crown—have been on display in the collection of secular and ecclesiastical treasures at the Hofburg Palace (now the Imperial Treasury Vienna).

Figure 6: This coloured copperplate print of the Imperial Crown of the Holy Roman Empire, by Johann Adam Delsenbach (1687–1765), was created around 1751 and released in 1790 as plate 1 of 'Wahre Abbildung der sämtlichen Reichskleinodien' (True representation of all imperial jewels). © KHM-Museumsverband, The Library, inv. no. 35.326I; reproduced with permission.

MATERIALS AND METHODS

The Imperial Crown is an object of inestimable value. It was, therefore, necessary that all analyses be done on-site and be fully non-destructive, without any opportunity to detach the gems from the crown or otherwise manipulate them. Consequently, it was necessary to use a portable spectrometer system. Basic requirements included an easily positionable detector head and—because of the fairly complex surface shape of the crown—a sufficiently large free working distance.

For spectroscopy, the parts of the Imperial Crown to be analysed (eight-plate circlet, cross and arch) were separately placed onto a turntable (Figure 7), and their positions were manually adjusted by qualified museum conservators. Spectroscopists were forbidden to touch the objects. Options available to visually inspect the stones included hand-held UV and white-light LED lamps, and a 407 nm laser pointer (the last being particularly suitable to excite Cr-related luminescence in gems; see Zeug *et al.* 2022). Analyses were assisted by high-resolution images of stones obtained with a Hirox HRX-01 3D digital microscope. The spectroscopic analyses were carried out over the course of eight working days in May 2022.

Laser-induced photoluminescence (PL) and Raman spectra were obtained using a fibre-coupled WITec confocal Raman probe system with an alpha300 controller. The system featured a probe head equipped with an Olympus 20× objective (numerical aperture 0.25, free working distance 25 mm), a WITec UHTS 300

VIS ultra-high throughput spectrometer (focal length 300 mm) and a Peltier-cooled Andor Newton EMCCD (electron-multiplying charge-coupled device) detector. The system was operated using WITec's Suite Six software. Spectra were excited with the 457 nm emission of a diode laser (using a power of 0.05–8.5 mW at the sample surface for PL measurements depending on the emission intensity, and 8.5 mW for Raman measurements). The use of a green laser (532 nm excitation) was not considered, as it is well known that Raman spectra of several coloured stones (especially corundum) are strongly obscured by luminescence in the green range. For PL analyses, we used a diffraction grating with 600 grooves/mm, yielding an approximate spectral resolution in the range of 5 cm^{-1} (red) to 4 cm^{-1} (nearest IR). The Raman-scattered light was analysed by means of a diffraction grating with 1,800 grooves/mm, resulting in a spectral resolution of 3 cm^{-1} (for blue light).

PL spectra were calibrated using lines of an Ar/Hg spectral lamp, and the accuracy of PL emissions in the red to near-infrared (NIR) range was better than ±0.03 nm. All Raman spectra obtained included a small part of the anti-Stokes region, and the position of the Rayleigh line (Raman shift 0 cm^{-1}) was used to check and adjust wavenumber calibration, resulting in an accuracy of Raman shifts better than ±0.5 cm^{-1}. After appropriate background correction, Raman spectra of spinels were fitted assuming asymmetric pseudo-Voigt shapes (Slotznick & Shim 2008). Fitted FWHM (full width at half band maximum) values were corrected for the artefact of experimental band broadening according to Váczi (2014).

To document and discuss the analytical results for the gemstones (Figure 8), we followed the internal sample labelling system of the Kunsthistorisches Museum Vienna, which consists of combinations of letters and digits. The eight plates of the circlet are labelled A to H, counter-clockwise when seen from the top, beginning with A for the front plate. Thus, the left temporal plate is designated C, the nape plate is E, and so on (again, see Figure 8). The cross is designated K for the German *Kreuz* (cross). The two sides of the arch are designated BgCh and BgRo, which are derived from (1) the German ***Bügel*** (arch) and (2) the first two letters of the inscriptions formed by several hundred small pearls: on the arch's left side '**CH**VONRADVS DEI GRATIA' and on the right side '**RO**MANORV[M] IMPERATOR AVG[VSTVS]'. For the sample label of each gemstone, the following digit refers to consecutive horizontal numbering, from left to right, of both gemstones and large pearls on each single object, from top to bottom.

Reference materials consisted of the following: a clear, pinkish red gem spinel (Ratnapura, Sri Lanka), three almandines (from Garibpet and Rajmahal, India, and a Sasanian engraved gem), a Ca-poor pyrope-almandine (a Roman engraved gem from the Helmut Hansmann collection, Staatliche Antikensammlung München, inv. no. NI-15.046-473), a Ca-rich pyrope-almandine bead (from Anuradhapura, Sri Lanka; no. 23 in Schüssler *et al.* 2001), a grossular (Kamburupitiya, Sri Lanka) and two graphite samples (crystalline from Kahatagaha, Sri Lanka, and disordered from Saskatchewan, Canada). As one of the spinels in the crown showed spectroscopic evidence of heating, and to systematically document the effects of heat treatment on the PL and Raman spectra of gem spinel, two chips from our reference sample were placed in a platinum crucible and heated (in air) at a rate of 30°C per minute to 700°C and 1000°C, respectively. After two hours, the furnace was then switched

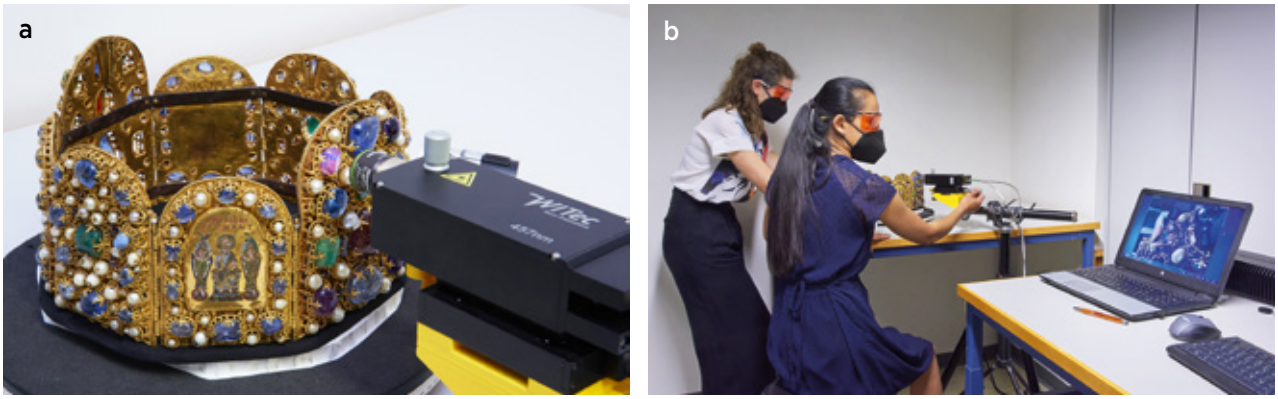

Figure 7: (**a**) The object (here the circlet after removal of the velvet biretta, arch and cross) was placed on a turntable in front of the position-adjustable probe head. Note the two inner, riveted iron strips that were mounted during an early modification phase of the crown to stabilise the octagon. (**b**) For Raman spectroscopy, the gem to be analysed was first roughly focused by minimising the laser spot seen in the video image, and then further focused by maximising the spectroscopic signal of interest. Shown here are authors CCN (right) and TL (left); they are wearing face coverings to protect the crown—especially its enamel figures—from the moisture of exhaled air. Photos © KHM-Museumsverband (Christian Mendez); reproduced with permission.

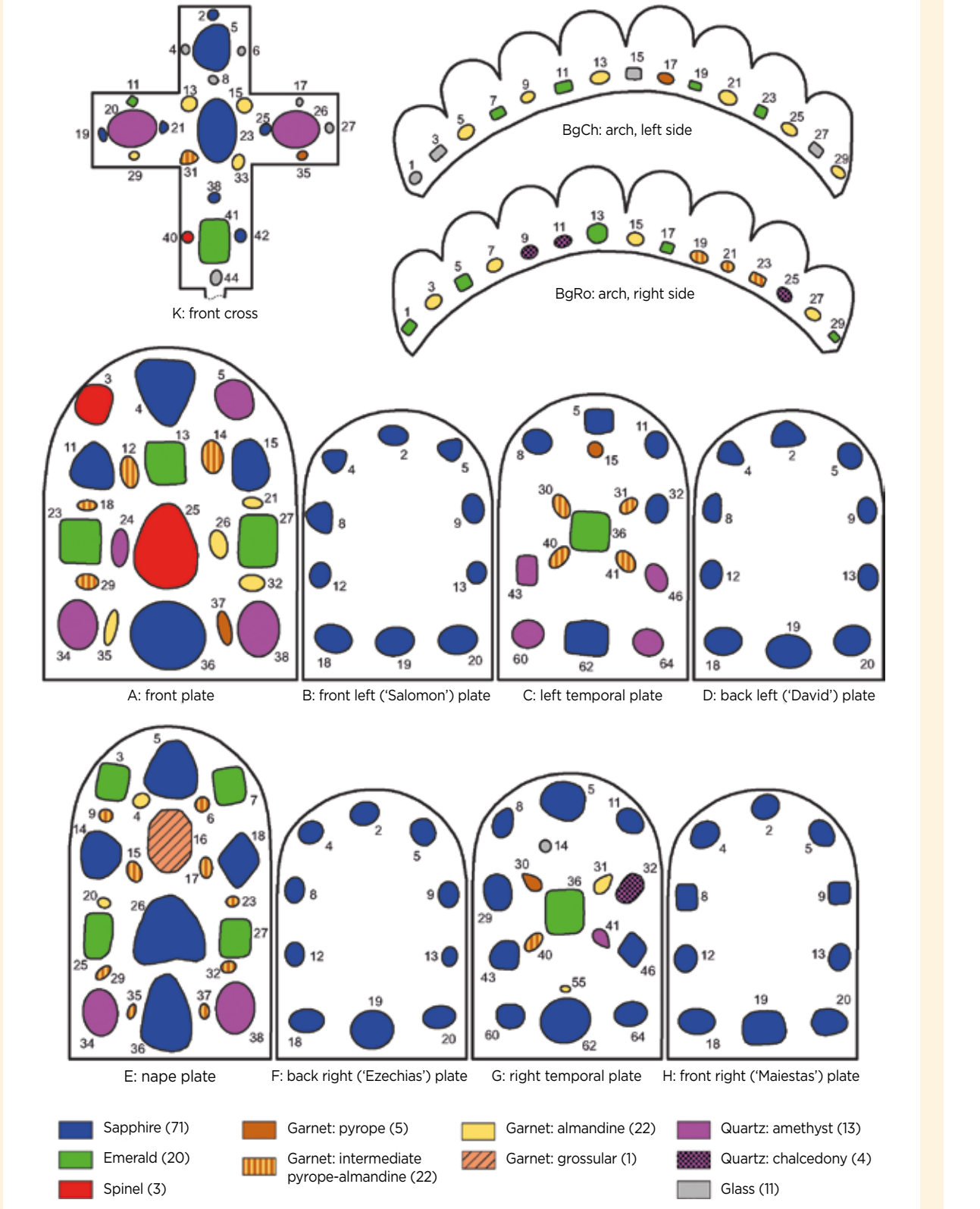

Figure 8: This drawing illustrates the distribution of the inorganic gem materials in the various components of the Imperial Crown, as identified in this study. For clarity and relevance to the present article, only inorganic gems are shown; pearls and enamelled areas are not indicated. The cross has been enlarged (by about 1.3×) relative to all other parts of the crown for clarity in labelling its many small stones. Sample numbers used throughout this article relate to the designations shown here.

off and each sample was allowed to cool down slowly (i.e. over several hours) in the closed furnace. To collect reference spectra, three spectrometers were used. Photoluminescence and Raman spectra with 473 nm excitation (0.42 and 17 mW, respectively) were obtained using a Horiba LabRAM HR Evolution system. With a diffraction grating of 1,800 grooves/mm in the beam path, the spectral resolution was in the range between 1.2 cm^{-1} (for blue light) and 0.6 cm^{-1} (NIR). Additional experimental details are described in Zeug *et al.* (2018). Raman spectra with 532 nm (14 mW) excitation were obtained using a Horiba XploRA Plus system equipped with a diffraction grating of 1,800 grooves/mm; for further details see Schmetzer *et al.* (2017). The garnet from Staatliche Antikensammlung München was analysed using a WITec alpha300 R Raman microscope with 532 nm (3.5 mW) excitation; more details are reported in Gilg and Gast (2012).

RESULTS AND DISCUSSION

Photoluminescence Analysis

More than half of the gemstones in the Imperial Crown yielded more-or-less intense PL in the red-to-NIR range of the electromagnetic spectrum. In many cases, the emission was easily seen with the unaided eye, especially upon illumination with the 407 nm laser pointer (Figure 9). Detection and analysis of such strong spectroscopic signals enabled a relatively uncomplicated study of the stones. In particular, the identification of sapphires—as corundum is a relatively poor Raman scatterer—became quite straightforward: depending on the respective emission intensity, laser-induced PL had a count rate between 25 times (stone G5) and 200,000 times (stone F18) higher, compared to the count rate of the main Raman band. Analysing a suspected sapphire by maximising the signal intensity of the red PL emission was thus considerably easier than relying on the Raman signal. The same procedure was used for suspected emeralds and spinels.

A total of 94 gemstones in the Imperial Crown (71 sapphires, 20 emeralds and three spinels; Figures 10–12) were identified from their characteristic PL spectra (Figure 13). Emissions of all three gem minerals are mainly related to Cr^{3+} (even though contributions of other emission centres, such as V^{2+}, need to be considered; cf. Ollier *et al.* 2015). The obvious differences in emission characteristics among the three gem minerals are due to different effects of the crystal field surrounding the Cr^{3+} ions (for a summary, see Box B in Zeug *et al.* 2022).

Figure 9: A large, transparent sapphire in the bottom centre of the circlet's right temporal plate (stone G62; 2.1 cm long) shows (**a**) vivid blue colour in ambient room lighting, but (**b**) intense pinkish red emission from a 407 nm laser pointer. Photos © KHM-Museumsverband (Christian Mendez); reproduced with permission.

Corundum has a fairly strong crystal field, resulting in a comparably large energy difference between the ^2E and $^4T_2$ excited levels. Direct $^4T_2 \rightarrow {}^4A_2$ electronic relaxation does not occur at room temperature. Instead, excited electrons undergo fast intersystem crossing from the $^4T_2$ to the split ^2E level (Kisliuk & Moore 1967). The emission is therefore dominated by spin-forbidden $^2E \rightarrow {}^4A_2$ relaxation, observed as two narrow *R* lines (Nelson & Sturge 1965) at 14405 and 14436 cm^{-1} (694.2 and 692.7 nm in Figure 13). Low-intensity PL features in the range 13500–15250 cm^{-1} (about 740–655 nm) are caused by vibronic sidebands (couplings of main emissions with lattice vibrations; Rothamel *et al.* 1983). The narrow *N* lines at 14203 and 14267 cm^{-1} (704.1 and 700.9 nm; analogues of *R* lines that are caused by closely spaced Cr^{3+} pairs; Powell *et al.* 1967) were not observed in our spectra. This is due to the generally low Cr^{3+} concentrations of the pale greyish blue (e.g. Figure 10a) to vivid blue (e.g. Figure 10b) sapphires. Emission patterns of all 71 sapphires were fairly similar, but with vast differences in absolute intensity, which might in first approximation be correlated to the Cr content in each gem. However, no general correlation between sample colour and emission intensity was observed, which reconfirms that the intensity of blue sapphire colouration is independent of Cr content.

The emission spectrum of beryl (Figure 13), with its comparatively weak crystal field, is dominated by a broad hump in the range 11500–15500 cm^{-1} (about 870–645 nm) that is assigned to spin-allowed $^4T_2 \rightarrow {}^4A_2$ electronic relaxation. This is superimposed by two low-intensity, quite broad *R* lines at 14615 and 14695 cm^{-1} (684.2 and 680.5 nm) that are due to the spin-forbidden $^2E \rightarrow {}^4A_2$ electronic transition (Kisliuk & Moore 1967; Ollier *et al.* 2015) of Cr^{3+} and/or V^{2+}. In our beryl spectra, total PL intensity and relative intensity of the *R* lines correlated with sample colour (Figure 13) and, hence, presumably with chemical composition. Pale green emeralds (such as BgRo29) yielded low-intensity PL with relatively clear *R* lines, whereas in the higher-intensity emission spectra of vivid green stones (such as E25; Figure 11a) the *R* lines were poorly resolved (again, see Figure 13). For the latter, the main hump was shifted notably towards lower wavenumbers (from

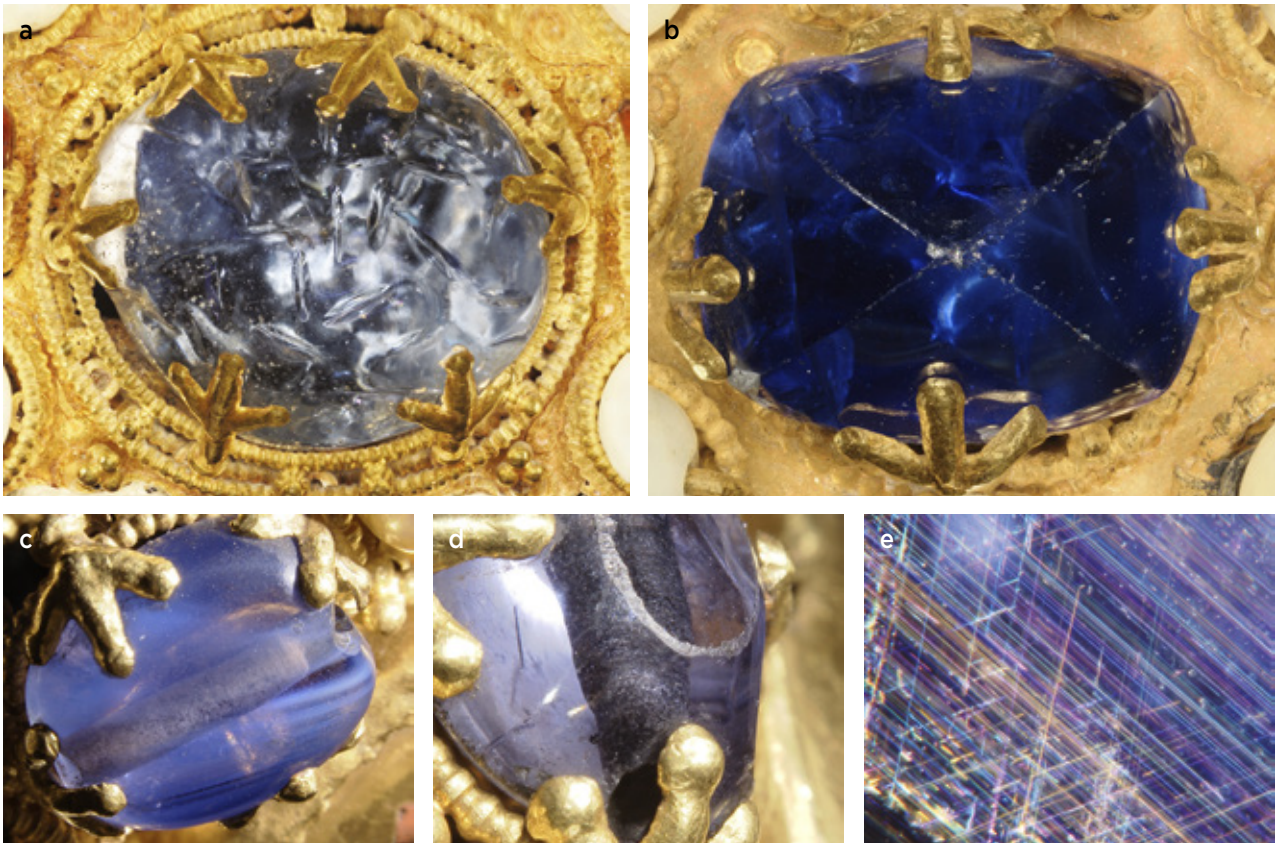

Figure 10: The sapphires in the crown range from (**a**) pale blue (stone A36, image width 4.0 cm) to (**b**) dark 'cornflower' blue (C62; image width 2.3 cm). (**c**) Many of the sapphires show growth zoning, as can be seen at lower right in this drilled cabochon (H4; image width 1.4 cm). (**d**) Drill-hole walls are, in some cases, coated with graphitic carbon (F8; image width 7.8 mm). (**e**) Oriented rutile needles such as these were seen in several of the sapphires (C5; image width 1.7 mm). Photos © KHM-Museumsverband (Herbert Reitschuler); reproduced with permission.

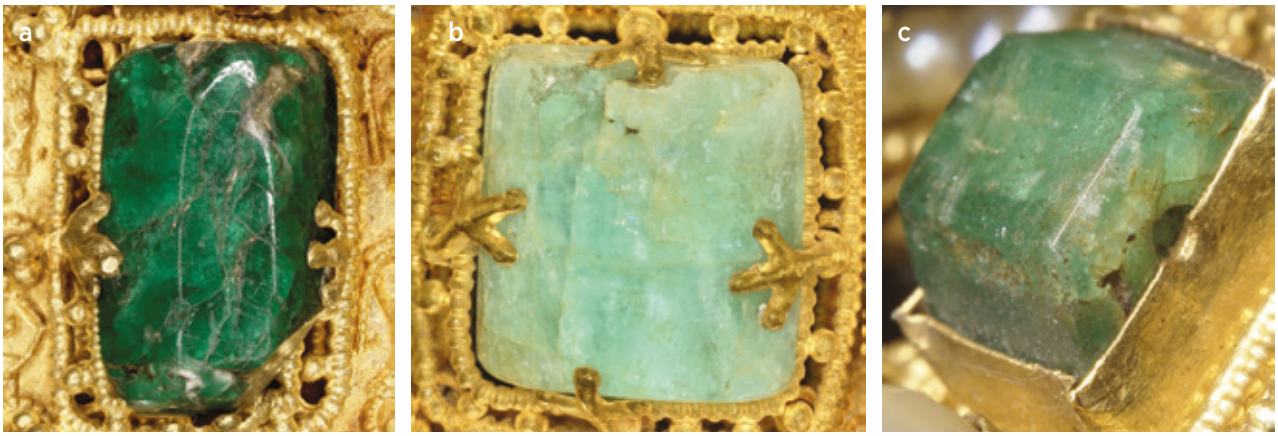

Figure 11: Emeralds in the crown range from (**a**) vivid green (stone E25; image width 1.9 cm) to (**b**) pale green (A23, image width 2.3 cm). (**c**) Some of the emeralds are only lightly polished and still exhibit a natural hexagonal prismatic crystal shape (BgCh23; image width 6.9 mm). Photos © KHM-Museumsverband (Herbert Reitschuler); reproduced with permission.

about 13750 to 13500 cm^{-1}, or about 727 to 741 nm), which could indicate an increased contribution of the $^4T_2 \rightarrow {}^4A_2$ electronic transition of V^{2+} (Ollier *et al.* 2015).

Similar to corundum, Mg-Al spinel has a rather high crystal-field strength, and the emission is therefore controlled by the spin-forbidden $^2E \rightarrow {}^4A_2$ electronic transition. However, compared to sapphire and emerald, the PL pattern of gem spinel is much more complex (Figure 13). For a summary description of the emissions, see Brik *et al.* (2016) and references therein. In addition to the *R* line near 14590 cm^{-1} (685.4 nm), there are several *N* lines, which are assigned to either Cr^{3+} pairs or cation perturbations in the host ('structure-dependent' *N* lines; Mikenda & Preisinger 1981). Both *R* and *N* lines have fairly strong vibrational couplings (Mohler & White 1995), generally referred to as phonon sidebands. All aforementioned spectral components sum up to a typical fingerprint pattern of emission features (again, see Figure 13) that enables straightforward spinel identification. The integral emission intensities in the red range obtained from the violet-to-pinkish red spinels A25 and A3 (Figure 12a, b) were similar, whereas reddish orange spinel K40 (Figure 12c) emitted about four times as much red light under comparable experimental conditions (laser power and measurement time).

Raman Analysis: General Results

Our identifications of all sapphires (for a reference spectrum, see Porto & Krishnan 1967), emeralds (Hagemann *et al.* 1990) and spinels (White & DeAngelis 1967) were confirmed by their Raman spectra (not shown). However, many Raman spectra were obscured by more-or-less intense background luminescence. This was especially the case for the vivid green emeralds (A13, A27, E25 and G36), which generated such strong background signals that it was impossible to obtain Raman spectra in the O–H stretching region (although the elevated background did not prevent mineral

Figure 12: There are only three spinels in the crown: two large specimens (**a**) A25 (image width 3.6 cm) and (**b**) A3 (image width 2.0 cm) mounted in the front plate, and (**c**) a small stone of rather low quality (K40; image width 4.7 mm) in the cross. Photos © KHM-Museumsverband (Herbert Reitschuler); reproduced with permission.

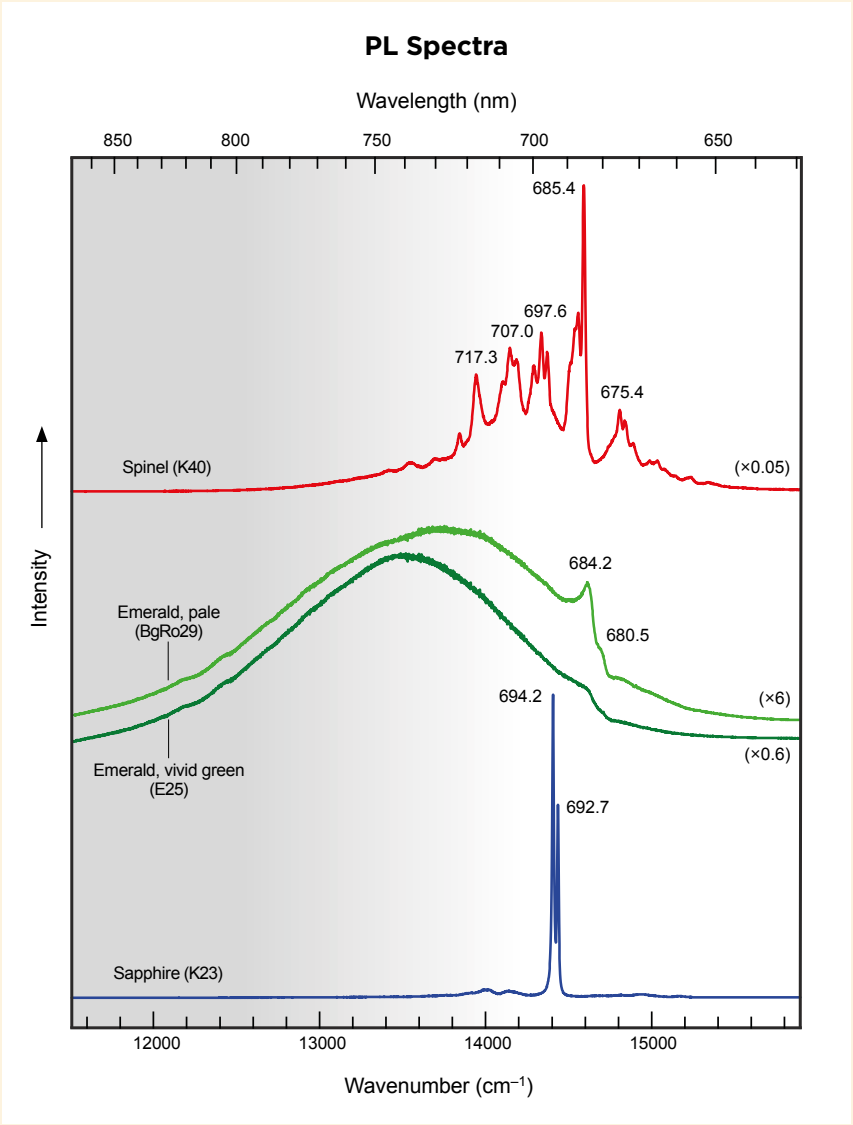

Figure 13: Representative PL spectra (457 nm excitation) are shown for three Cr-containing gem minerals in the Imperial Crown: sapphire, emerald (pale and vividly coloured examples) and spinel. The spectra are offset vertically for clarity, and the emission intensity of the spectrum of stone K23 (one of the lowest-PL sapphires in this study) was adjusted for clarity and comparison. The NIR spectral range not visible to the human eye is shaded grey.

identification in the Raman shift range of 100–1200 cm^{-1}). Water bands could only be identified in some of the low-luminescence, pale-coloured emeralds (such as C36 and E7). Here, the O–H stretching range (again, not shown) is dominated by a symmetric band at 3597 cm^{-1}, which is assigned to 'type II water' (Huong *et al.* 2010); that is, water molecules adjacent to alkali ions in structural channels. Consequently, these pale emeralds originated from alkali-rich 'schist type' deposits.

The remaining 78 stones in the crown were identified only from their Raman spectra. They included 11 glass, 17 quartz and 50 garnet specimens.

The glass gems in the Imperial Crown (e.g. Figure 14) were presumably selected by goldsmiths according to colour, to imitate more valuable gems. Colours span the wide range from vivid green (K4, BgCh3, BgCh15 and BgCh27), pale green (K17), deep bluish green (K6) and greenish blue (K8); vivid blue (K27 and K44); and red (G14) to dark brownish red (BgCh1). Obtaining Raman spectra from the glass specimens was challenging. Glass has a much lower Raman-scattering intensity than most crystalline gem materials, and the poor signal was typically overlain by weak-to-strong background phenomena (in some cases including intense luminescence of material underlying the stones in the settings). Adjusting the probe head position in order to maximise the low-intensity Raman signal was, therefore, tedious and time-consuming. Even though the identity of the glasses had been suspected from bubble-like inclusions observed with the optical microscope, it was desirable to provide positive spectroscopic evidence of their identity. All these stones yielded spectra (not shown) dominated by a broad double band or plateau at 950–1100 cm^{-1} (several stretching modes) and a broad band at 550–620

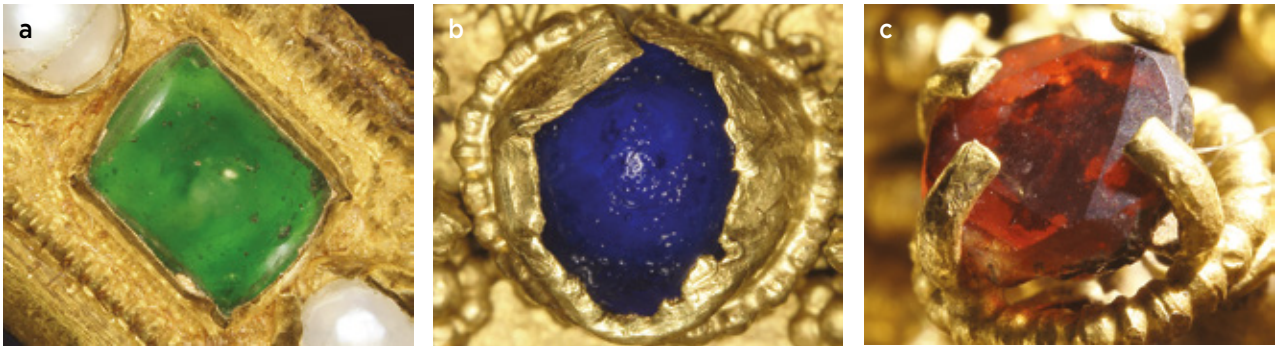

Figure 14: Three of the 11 glass gems in the crown are shown here: (**a**) BgCh27 (image width 1.2 cm), (**b**) K44 (image width 7.7 mm) and (**c**) G14 (image width 6.4 mm). Photos © KHM-Museumsverband (Herbert Reitschuler); reproduced with permission.

cm^{-1} (bending), which characterises them as silicate glasses (Colomban 2003; Colomban *et al*. 2006; Neuville 2006).

Quartz samples consisted of 13 amethysts of diverse transparencies and hues, and four chalcedonies (e.g. Figure 15). Raman spectra of amethysts K26 and C60 were obscured by a flat background that increased towards higher Raman shifts; the background intensity depended quite strongly on the focused sample point. This phenomenon is rather unusual for macro-crystalline amethyst, and we attribute it to luminescence arising from foreign material (such as tissue, foil or glue) underlying the stones. The occasional presence of such material is supported by the observation that stone K26 resembled rose quartz or carnelian with white-light LED illumination from the front, but when illuminated from the side it appeared pale lilac. Its pink-to-brownish

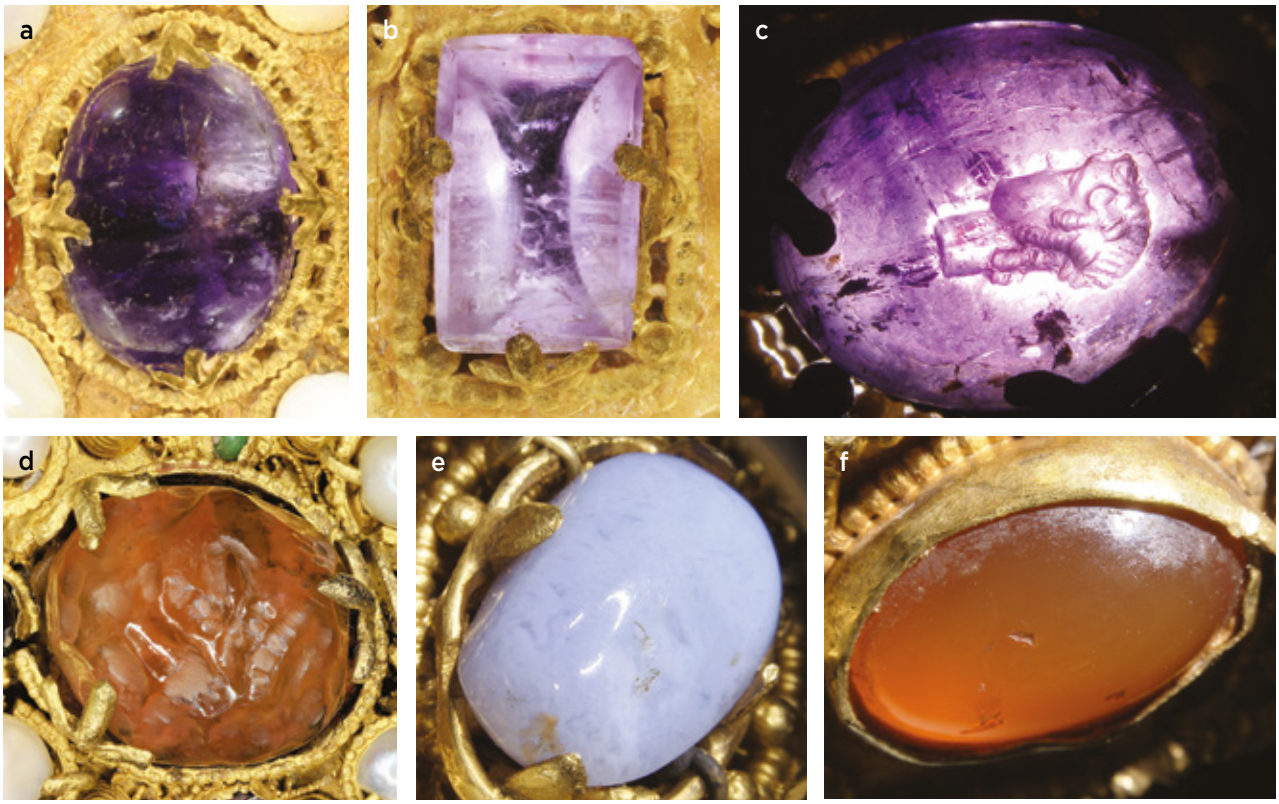

Figure 15: Quartz-family gems in the crown consist of amethyst and chalcedony. Most of the amethysts are (**a**) cabochons (stone A38; image width 2.4 cm) or (**b**) have a rectangular shape (C43; image width 1.2 cm). (**c**) Amethyst C64 at the lower left corner of the left temporal plate, seen here in transmitted light, consists of an intaglio showing the head of Apollon (image width 1.4 cm). (**d**) In spite of its appearance, stone K26 is not carnelian or rose quartz but rather very pale amethyst with a colour appearance that comes from an underlying reddish substance (image width 1.9 cm). (**e**) This pale bluish, milky chalcedony (G32; image width 1.2 cm) has a non-fitting prong setting in an apparent 'sapphire place' in the right temporal plate, which suggests it is a replacement. The three other chalcedonies are bezel-set in the arch's right side; two are pale greenish grey and (**f**) one has carnelian colour (BgRo11; image width 9.4 mm). Photos © KHM-Museumsverband (Herbert Reitschuler); reproduced with permission.

colouration seemed to come from a waxy reddish substance behind the stone. (For the assignments of quartz bands, see Etchepare *et al.* 1974.)

The chalcedonies were orange (carnelian BgRo11), milky white (G32) and an almost emerald-like pale greenish grey (BgRo9 and BgRo25). Their spectra (not shown) were all somewhat affected by background signal. In Raman spectra, fibrous chalcedony is distinguished from macro-crystalline quartz by an additional band at 502–503 cm^{-1} that is assigned to a combination of the main band of moganite (a monoclinic SiO_2 polymorph commonly occurring in chalcedony) and chemically bound water forming silanol (SiOH) groups (Schmidt *et al.* 2014).

Although the main objective of our first analytical campaign was the unequivocal identification of all inorganic gem materials in the crown, a few attempts were made to identify large, near-surface inclusions and accompanying phases, mainly based on high-resolution images of individual stones. Several of the sapphires had been used in other jewellery before being set in the Imperial Crown, as indicated by drill holes. One such hole in a sapphire contained a black substance covering its inner wall (Figure 10d), which was found to be strongly disordered graphitic carbon (Figure 16a; cf. Beyssac & Lazzeri 2012).

Whitish to pale grey inclusions in the emeralds were identified as apatite (Klee 1970) and Mg and Ca-Mg carbonate (Rividi *et al.* 2010). The two carbonate spectra (not shown) differed especially in the low-energy range comprising translational (around 200 cm^{-1}) and librational (around 300 cm^{-1}) external cation-carbonate vibrations.

Another interesting finding was a fairly strong band pattern in the Raman spectrum of the pale green glass K17 (Figure 16b). A similar pattern (although of lower intensity) was also detected in the dark bluish green glass K6. This spectrum matches the Raman pattern of a pigment known as 'lead tin yellow type II' (cubic $PbSn_{1-x}Si_xO_3$; Šefců *et al.* 2015), although another pigment called 'Naples yellow' (cubic $Pb_2Sb_2O_7$; Bell *et al.* 1997; Antušková *et al.* 2022) cannot be excluded at this time.

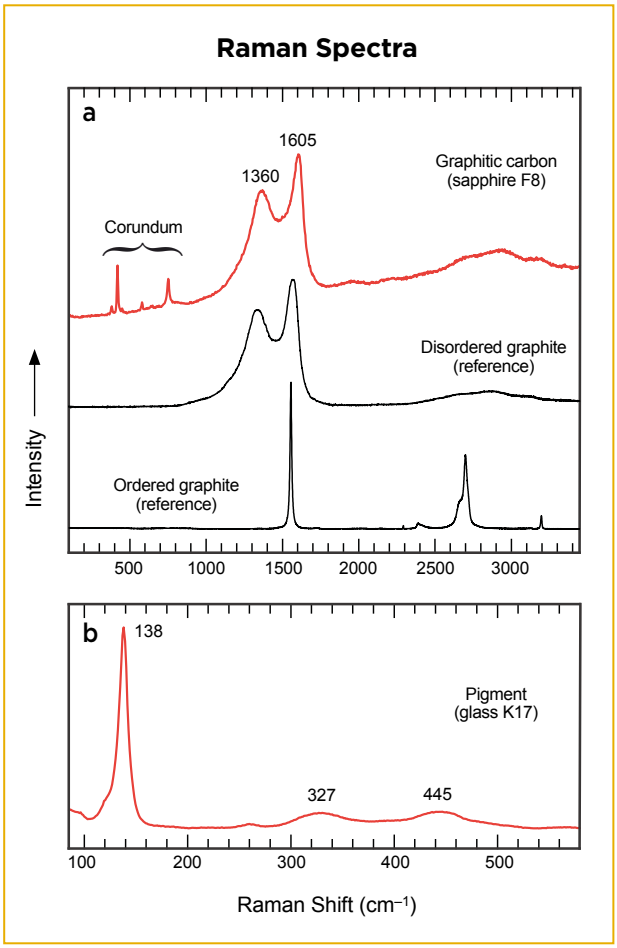

Figure 16: Selected Raman spectra (457 nm excitation) are shown for (**a**) a black substance in the borehole of sapphire F8, which consists of disordered sp^2 (graphitic) carbon (reference spectra were obtained with 473 nm excitation), and (**b**) the pigment in the pale whitish green glass K17, which is assigned to 'lead tin yellow type II'.

Raman Analysis: Garnets

In discussing Raman spectra of garnets, we use the band numbering system (from I to XVI) of Pinet and Smith (1994). For band assignments, see Hofmeister and Chopelas (1991) and Kolesov and Geiger (1998). For possible provenance assignments of garnets, the A–G cluster system of Then-Obłuska *et al.* (2021) is used here. Cluster assignments are based on chemical composition, which in turn influences Raman spectral characteristics and observed inclusion assemblages. Abbreviations of mineral names are from Whitney and Evans (2010).

Among the garnets in the Imperial Crown, 49 were members of the binary pyrope-almandine system, $(Mg,Fe^{2+})_3Al_2(SiO_4)_3$ (no spessartine was found), and only one was grossular, $Ca_3Al_2(SiO_4)_3$ (Figure 17). The 49 Mg-Fe garnets showed some variations in colour, Raman spectra and inclusions. Most of them were vivid red to reddish brown to dark brownish red (such as C40; Figure 17a), with only a few having lighter colouration (such as brownish yellow A14 or pink E32; Figure 17b). Most of the Raman spectra of Mg-Fe garnets (45 out of 49) could be classified into seven distinct categories: four types of almandine (Alm 1 to Alm 4), two types of intermediate pyrope-almandine (Prp-Alm 1 and Prp-Alm 2) and one type of pyrope (Prp; see Figure 18 and Table I). These different garnet types also showed distinct inclusion characteristics (Figures 19 and 20; Table II). The Raman

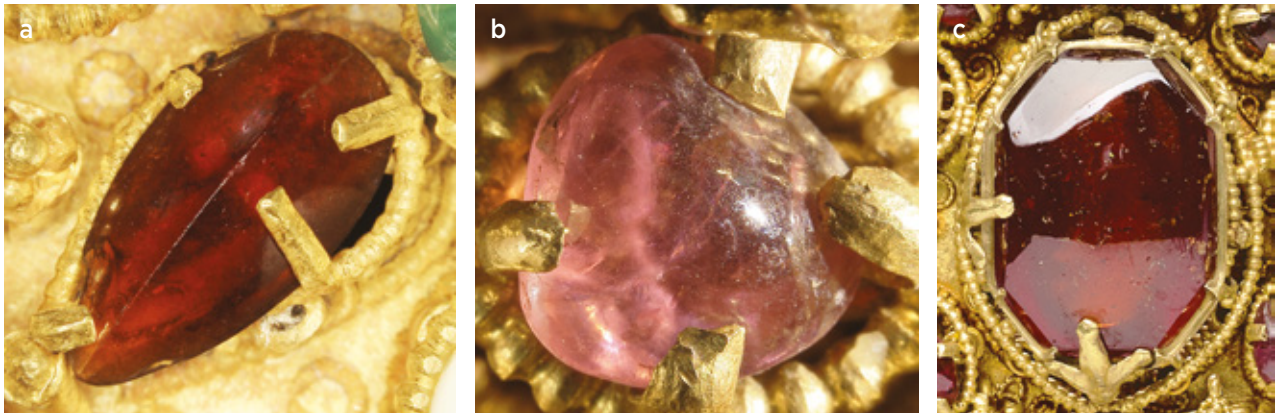

Figure 17: Almost all garnets in the crown belong to the pyrope-almandine series. Most commonly they are (**a**) vivid red to reddish brown (C40; image width 11.8 mm), but (**b**) a few show lighter colour (E32; image width 6 mm). (**c**) A single garnet in the crown, in the centre of the nape plate, is grossular—a large, well-polished stone of octagonal shape (E16, image width 3.2 cm). Photos © KHM-Museumsverband (Herbert Reitschuler); reproduced with permission.

band positions and observed inclusion characteristics of these types match those of garnets used in jewellery from the Hellenistic period to late antiquity (e.g. Rösch *et al.* 1997; Schüssler *et al.* 2001; Calligaro *et al.* 2002; Gilg *et al.* 2010; Gilg & Gast 2012; Thoresen & Schmetzer 2013; Gilg & Gast 2016; Schmetzer *et al.* 2017; Gilg *et al.* 2018; Kos *et al.* 2020; Then-Obłuska *et al.* 2021). Only four garnets (A14, C31, BgRo19 and BgRo21) yielded Raman band positions located between these seven types, and hence have intermediate chemical compositions.

The positions of the Raman bands in the various garnet types are summarised in Table II. Low Raman shifts of band V (F_{2g} mode related to SiO_4 bending) below 636 cm^{-1} and of band XII (A_{1g} mode related to rotations) below 349 cm^{-1} are indicative of almandine-rich garnets, while values above 639 and 355 cm^{-1}, respectively, characterise pyrope-rich compositions (Pinet & Smith 1994). Both bands are barely affected by additional spessartine (Mn) and grossular (Ca) components. By contrast, the spectral positions of band IV (F_{2g} mode related to Si–O stretching) and the intense band II (A_{1g} mode related to Si–O stretching) are both strongly shifted to lower wavenumbers by increasing grossular content. For these two bands, moderate spessartine and pyrope components in almandine-rich garnets have minimal effects. For instance, moderate spessartine contents of < 15 mol.%—corresponding to less than 6.5 wt.% MnO—influence these Raman bands for almandine by less than 1 cm^{-1}.

Orange-red almandine A35, the only representative of type Alm 1, showed significantly lower values for bands II and IV (913 and 857 cm^{-1}) than the other three almandine types Alm 2 to Alm 4 (Table II), suggesting a significantly higher Ca content. This garnet also showed a weak shoulder in the 830 cm^{-1} region that has been attributed to elevated Ti contents (Gilg & Gast 2016). It had no visible solid inclusions, only a single partially healed fracture (Figure 19a). The Raman spectral features of A35 (Figure 18a) match those of Ca-rich almandine in Roman engraved gemstones (cluster Z of Gilg & Gast 2012, recently renamed cluster F by Then-Obłuska *et al.* 2021). Cluster F garnets are orange-red, Ca-rich (4.7–7.7 wt.% CaO), Mg-poor (< 3 wt.% MgO) and have moderate TiO_2 contents of 0.03–0.12 wt.% (Gartzke 2004; Gilg & Gast 2012; Thoresen & Schmetzer 2013). They typically have partially healed fractures (Figure 19b) with secondary fluid inclusions, and only very rarely contain solid inclusions such as zircon or opaque phases (Gilg & Gast 2012; Thoresen & Schmetzer 2013, their group 4). Ca-rich almandine garnets of cluster F have so far only been described from objects dating from the third century BCE to the first century CE (Thoresen & Schmetzer 2013), and are absent from garnet cloisonné jewellery from late antiquity (e.g. Calligaro *et al.* 2002; Gilg *et al.* 2010). In addition, the shape of almandine A35 resembles curved garnets used in Heracles knots in diadems of the Hellenistic period (see figure 1 in Thoresen & Schmetzer 2013). The chemical composition of cluster F garnets is similar to those of the gem almandine from deposits mined in the nineteenth century in Zillertal, Austria, but cluster F stones lack the solid inclusions that characterise Austrian garnets (Leute 2000; Gilg & Gast 2012; Gilg & Hyršl 2014). The origin(s) of cluster F garnets is/are as yet unknown.

Three almandines (A21, G31 and K33) belong to type Alm 2. They had similarly low Raman shifts of band V compared to Alm 1, likewise inferring low Mg contents. Low Ca values are indicated by the spectral positions of bands II and IV (Table II). There are well-distinguishable bands XI at 370–371 cm^{-1} and XIII at

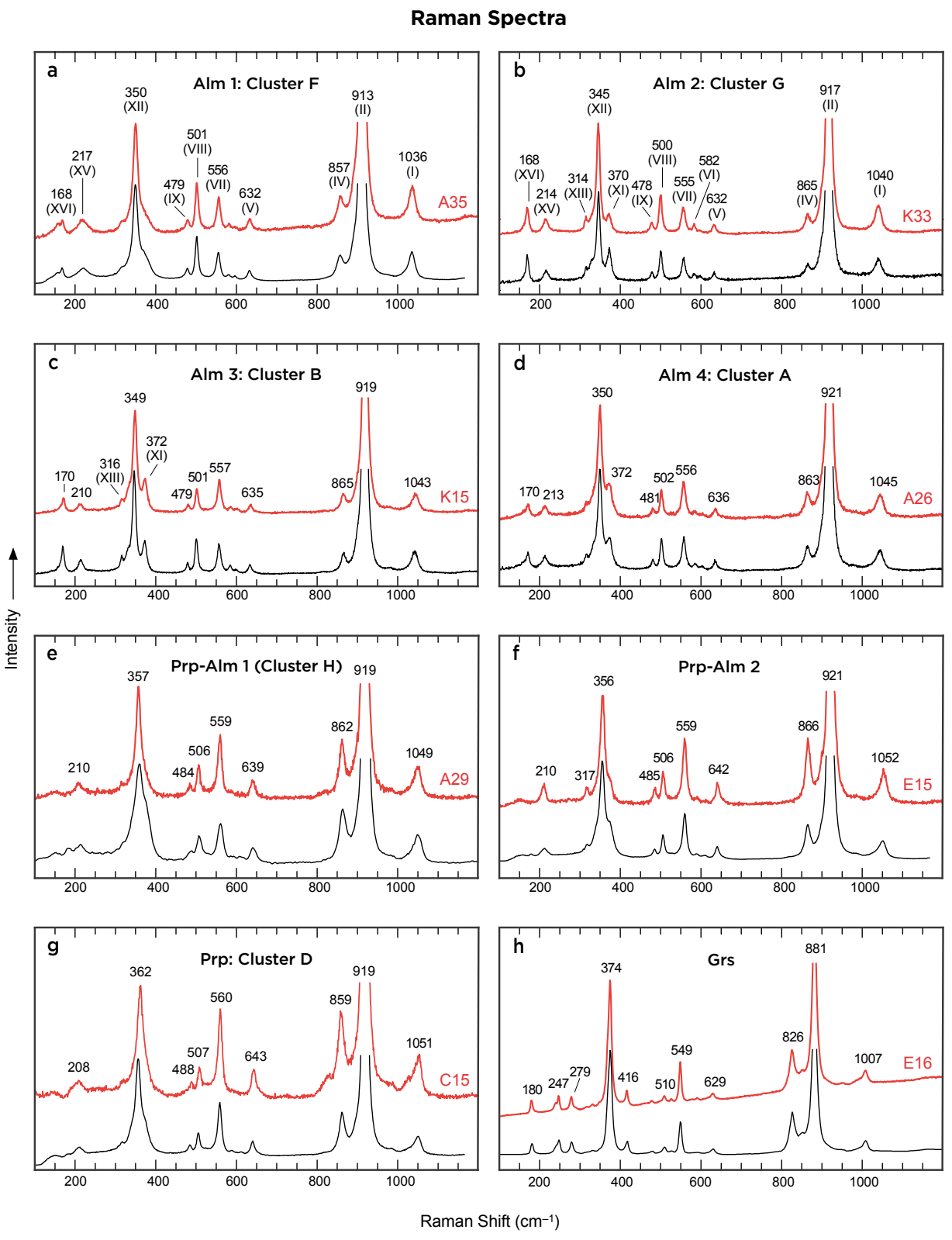

Figure 18: Representative Raman spectra of the different types of garnets in the crown (red traces) are compared to reference spectra (black traces) that were obtained from the following: (**a**) a Roman engraved gem (sample SL637 from Gilg & Gast 2012); (**b**) a cluster G almandine from the Garibpet deposit, Telangana State, India; (**c**) an almandine from Rajmahal, India; (**d**) a Sasanian engraved almandine; (**e**) a Ca-rich almandine-rich pyrope from Anuradhapura, Sri Lanka (i.e. 'cluster H', a designation that is still unpublished); (**f**) a low-Ca pyrope (Roman engraved gem); (**g**) a cluster D pyrope (Roman engraved gem; spectrum SL630 from Gilg & Gast 2012); and (**h**) a hessonite from Kamburupitiya, Sri Lanka. Spectra are offset vertically for clarity.

314–315 cm^{-1} (Figure 18b). These zoned garnet crystals had an inclusion-rich core with opaque and transparent long-prismatic crystals surrounded by abundant fibrous needles at the boundary with an inclusion-poor rim (Figure 19c). Their Raman spectra and inclusion characteristics match those of garnets from the Garibpet deposit, Telangana State, India (Figures 18b and 19d; Schmetzer *et al.* 2017). Garnets from this deposit are represented by (1) those used for bead production at Arikamedu, Tamil Nadu, India (Schmetzer *et al.* 2017), (2) beads recovered from Angkor Borei in Cambodia (Carter *et al.* 2021), (3) garnets in Hellenistic jewellery from northern Greece (Gartzke 2004) and (4) an Early Byzantine engraved gem (Gilg *et al.* 2018). This well-characterised garnet type was used from the second century BCE to the first millennium CE, and was termed cluster G by Then-Obłuska *et al.* (2021).

Garnets of types Alm 3 and Alm 4 were the most common almandine types in the Imperial Crown (14 and four gemstones, respectively). Their Raman band positions were widely overlapping, indicating similarly Ca-poor chemical compositions (Table II). Their spectra were differentiated only by slightly higher positions of bands XII and I (F_{2g} mode related to Si–O stretching) for Alm 3 (Figure 18c, d). This suggests a slightly higher pyrope content for Alm 4 (Pinet & Smith 1994). The inclusion assemblages of Alm 3 and Alm 4, however, were quite distinct. Alm 3 garnets were often inclusion-poor, but occasionally they had anhedral elongated slightly greenish inclusions up to 1 mm, small zircons with tension cracks (Figure 19e, f) and tiny spherical black inclusions with brownish radiation haloes (not shown), while Alm 4 garnets (cluster A) had a well-developed three-dimensional network of rutile needles, and opaque as well as rounded transparent inclusions (Figure 19g, h).

The inclusion assemblages and Raman band positions of Alm 3 and Alm 4 are identical to those observed for the two most prominent garnet varieties used in cloisonné jewellery of the Early Middle Ages: type I and type II of Calligaro *et al.* (2002), and cluster B and cluster A (Gilg *et al.* 2010, 2018; Kos *et al.* 2020), respectively. The almandines of cluster B appeared for the first time during the fifth century CE (Calligaro *et al.* 2002; Bugoi *et al.* 2016), while cluster A garnets have been known since

Table I: Assignment of the 50 garnets in the Imperial Crown.

Location	Sample	Assignment[a]	Cluster
Front plate	A12	Prp-Alm 1 (high Ca)	(H)[b]
	A14	Prp-Alm	
	A18	Prp-Alm 2 (low Ca)	
	A21	Alm 2	G
	A26	Alm 4	A
	A29	Prp-Alm 1 (high Ca)	(H)
	A32	Alm 3	B
	A35	Alm 1	F
	A37	Prp	D
Left temporal plate	C15	Prp	D
	C30	Prp-Alm 2 (low Ca)	
	C31	Prp-Alm	
	C40	Prp-Alm 1 (high Ca)	(H)
	C41	Prp-Alm 2 (low Ca)	
Nape plate	E4	Alm 3	B
	E6	Prp-Alm 1 (high Ca)	(H)
	E9	Prp-Alm 1 (high Ca)	(H)
	E15	Prp-Alm 2 (low Ca)	
	E16	Grs	
	E17	Prp-Alm 2 (low Ca)	
	E20	Alm 4	A
	E23	Prp-Alm 1 (high Ca)	(H)
	E29	Prp-Alm 1 (high Ca)	(H)
	E32	Prp-Alm 2 (low Ca)	
	E35	Prp-Alm 1 (high Ca)	(H)
	E37	Prp-Alm 1 (high Ca)	(H)
Right temporal plate	G30	Prp	D
	G31	Alm 2	G
	G40	Prp-Alm 2 (low Ca)	
	G55	Alm 4	A
Cross	K13	Alm 4	A
	K15	Alm 3	B
	K29	Alm 3	B
	K31	Prp-Alm 1 (high Ca)	(H)
	K33	Alm 2	G
	K35	Prp	D
Arch, left side	BgCh5	Alm 3	B
	BgCh9	Alm 3	B
	BgCh13	Alm 3	B
	BgCh17	Prp	D
	BgCh21	Alm 3	B
	BgCh25	Alm 3	B
	BgCh29	Alm 3	B
Arch, right side	BgRo3	Alm 3	B
	BgRo7	Alm 3	B
	BgRo15	Alm 3	B
	BgRo19	Prp-Alm	
	BgRo21	Prp-Alm	
	BgRo23	Prp-Alm 2 (low Ca)	
	BgRo27	Alm 3	B

[a] Abbreviations of mineral names (Alm = almandine, Grs = grossular and Prp = pyrope) are according to Whitney and Evans (2010).
[b] Cluster H is hitherto still unpublished (Gilg *et al.*, in preparation), and is therefore shown in parentheses.

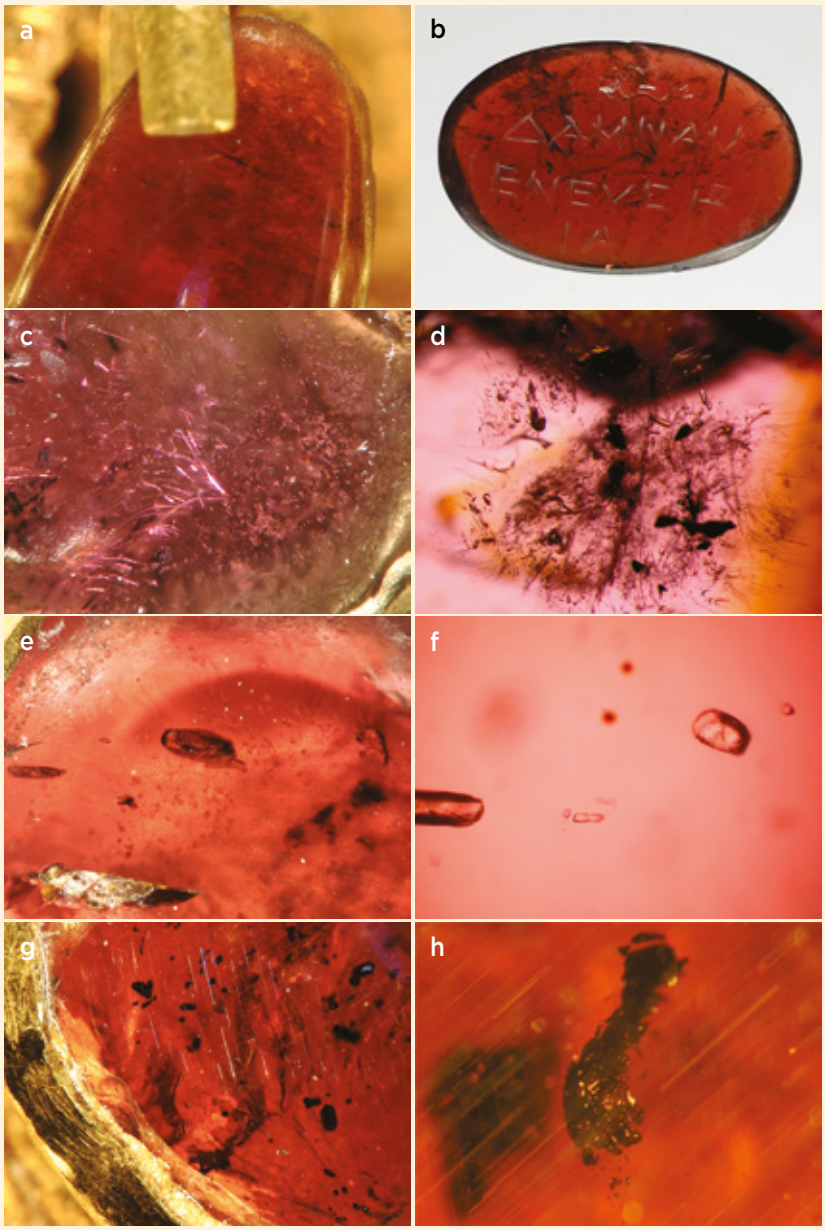

Figure 19: Inclusions in almandines of the crown are shown with comparison samples. (Note that inclusion minerals were identified by Raman spectroscopy only in the comparison samples.) Partially healed fractures, but no mineral inclusions, are present in (**a**) stone A35 (image width 5.3 mm) and in (**b**) a comparison almandine (cluster F; Roman engraved gem from Staatliche Antikensammlung München, inv. no. NI 15.046-101; 1.84 cm tall). Sillimanite fibres and inclusion zoning are present in (**c**) K33 (image width 2.3 mm) and in (**d**) a comparison almandine from Garibpet (image width 3.2 mm). Apatite inclusions can be seen in (**e**) K33 (image width 2.9 mm) and in (**f**) a cluster B almandine from Nordendorf, Germany, the latter also with tiny uraninite inclusions (image width 75 µm). Rutile needles and ilmenite are present in (**g**) A26 (image width 1 mm) and in (**h**) a cluster A almandine from Unterhaching, Germany (image width 1.3 mm). Photomicrographs a, c, e and g © KHM-Museumsverband (Herbert Reitschuler); reproduced with permission. Photomicrographs b, d and f by H. A. Gilg, and h by Norbert Hommrichhausen.

the Hellenistic period (Gartzke 2004; Gilg & Gast 2012; Thoresen & Schmetzer 2013). Garnets with chemical compositions similar to both of these types were found in a reliquary crown from Namur, Belgium, dated from the early thirteenth century (Bruni *et al.* 2021), and also in fourteenth century jewellery in Germany (Greiff 2010). Inclusion observations supporting the attribution to the garnet types, however, were not reported in these studies. Cluster B garnets were very probably sourced from the Rajmahal District, Rajasthan, India, while the provenance of cluster A garnets is still unclear (Gilg *et al.* 2019).

Two types of intermediate pyrope-almandine (Prp-Alm 1 and Prp-Alm 2) could be distinguished on the basis of their Raman band positions. The overlapping values of their bands V and XII suggest that they have similar Mg contents that are higher than that of the four Alm types. Low Raman shifts of bands II and IV of Prp-Alm 1 indicate higher Ca content than for Ca-poor Prp-Alm 2 (Figure 18e, f; Table II). The Raman band positions of Prp-Alm 1 are identical to those of garnet beads and rough stones excavated from archaeological sites dating to the first millennium CE in Sri Lanka (Rösch *et al.* 1997; Schüssler *et al.* 2001) and a third- to fourth-century CE ring stone in the James Loeb collection (SL630 in Gilg & Gast 2012). Their Ca-rich (3.9–6.1 wt.% CaO) compositions, with pyrope and almandine contents varying between about 30 and 55 mol.% (Rösch *et al.* 1997;

Table II: Raman shifts of main bands, inclusions and cluster assignment for 45 of the 49 Mg-Fe garnets in the Imperial Crown.

Garnet type	Alm 1	Alm 2	Alm 3	Alm 4	Prp-Alm 1	Prp-Alm 2	Prp
No. samples	1	3	13	5	10	8	5
Raman shifts (cm^{-1})							
Band I	1036	1039–1040	1040–1043	1044–1045	1049–1052	1051–1055	1049–1051
Band II	913	916–917	917–919	917–919	918–919	921–924	917–919
Band IV	857	864–865	864–866	863–866	861–862	865–867	859–860
Band 830*	Shoulder	–	–	–	–	–	Shoulder
Band V	632	631–633	632–635	633–636	639–641	640–643	641–643
Band VII	556	555	556–558	556–558	557–559	559–561	559–560
Band VIII	501	498–500	500–502	501–502	506–507	505–508	506–508
Band IX	479	476–478	478–480	479–481	484–485	485–487	487–488
Band XI	Shoulder	370–371	370–372	370–372	Shoulder	373–375	Shoulder
Band XII	350	344–345	345–347	348–349	356–357	355–357	358–362
Band XIII	Shoulder	314–315	314–317	315–316	Shoulder	317–318	Shoulder
Band XV	217	214	210–214	210–216	209–210	209–210	208–210
Band XVI	168	167–168	168–170	169–171	–	–	–
Colour	Orange-red	Red to violet	Brownish red to pink	Orange-red to brownish red	Red to dark red	Red to violet/pink	Orange-red to dark red
Inclusions	No solid inclusions; healed fractures	Zoned: inclusion-rich core with ilmenite, prismatic apatite and sillimanite bundles at boundary to inclusion-poor rim	Inclusion-poor: anhedral apatite, uraninite, zircon	Inclusion-rich: rutile needles, ilmenite, quartz, sillimanite, zircon	Inclusion-rich: oriented short needles and short prismatic crystals ('dashes and dots')	Inclusion-rich: oriented needles and short prismatic crystals ('dashes and dots'), clusters of roundish apatite	No inclusions
Garnet cluster	F	G	B	A	(H)	–	D

* This band has remained unnamed (Pinet & Smith 1994).

Schüssler *et al.* 2001; Gilg & Gast 2012), mark a narrow area within the large field of un-clustered garnet compositions in cloisonné jewellery (Gilg *et al.* 2010), or type III of Calligaro *et al.* (2002). Abundant equant to needle-shaped mineral inclusions ('dashes and dots'), with preferred orientations forming a loose three-dimensional network, are found in both Prp-Alm 1 garnet and in Sri Lankan garnet beads (Figure 20a, b). The same oriented equant to needle-shaped mineral inclusions and rarely clusters of rounded transparent crystals (Figure 20c, d) were observed in the Ca-poor Prp-Alm 2 garnets.

The five orange-red inclusion-free pyropes (type Prp, e.g. Figure 20e) were characterised by the lowest positions of band IV (859–860 cm^{-1}), the highest Raman shifts of band XII (358–362 cm^{-1}) and a significant shoulder in the 830 cm^{-1} region, indicating a Ca-, Mg- and Ti-rich composition (see Table II and Figure 18g). The Raman spectra of these five pyropes match those of the orange-red inclusion-free (e.g. Figure 20f) Cr-poor, Ti-rich pyropes of cluster D (Gilg & Gast 2012, 2016; Then-Obłuska *et al.* 2021), but are distinct from the red-to-violet Cr- and Ti-rich and more Mg-rich Bohemian pyropes (Gilg & Hyršl 2014; Gilg & Gast 2016). Cluster D pyropes have been used since the Hellenistic period and form phenocrysts in alkaline basaltic rocks. Such a geological provenance can be inferred for type Prp in the present study, as all known occurrences have overlapping chemical compositions. Potential sources in antiquity and the medieval

period are Monte Suímo in Portugal, alluvial deposits in Jos and the Biu plateau in northern Nigeria, Mount Carmel in Israel and Elie Ness in Scotland (Then-Obłuska *et al.* 2021).

Interestingly, the only grossular in the crown (the large octagonal, vivid orange to brownish red stone E16 on the nape plate; Figure 17c) is not original but was a replacement. The original stone was lost after a treasurer pressed the pillowed crown firmly to his body while riding to the royal quarters, and in 1764 the empty setting was filled with an assumed-to-be 'jacinth' (Klaar 1986) from a necklace. In 1977, based only on visual inspection, Prof. Kurat of the Natural History Museum Vienna correctly recognised that this stone could not be a zircon and identified it as a red garnet (see Figure 5). The very low Raman shifts of bands II and IV (826 and 881 cm^{-1}; Figure 18h) are very close to the respective end-member values of grossular (Kolesov & Geiger 1998). The assignment to 'hessonite' is supported by the common presence of transparent rounded inclusions (probably apatite and/or calcite; Figure 20g, h), the stone's orange-brown colour and its 'oily' diaphaneity (Mathavan *et al.* 2000).

The Enigma of Spinel A25

Natural Mg-Al spinel of gem quality typically yields PL and Raman fingerprint patterns analogous to those of stone K40 (Figures 12c and 13). Such spectra were also

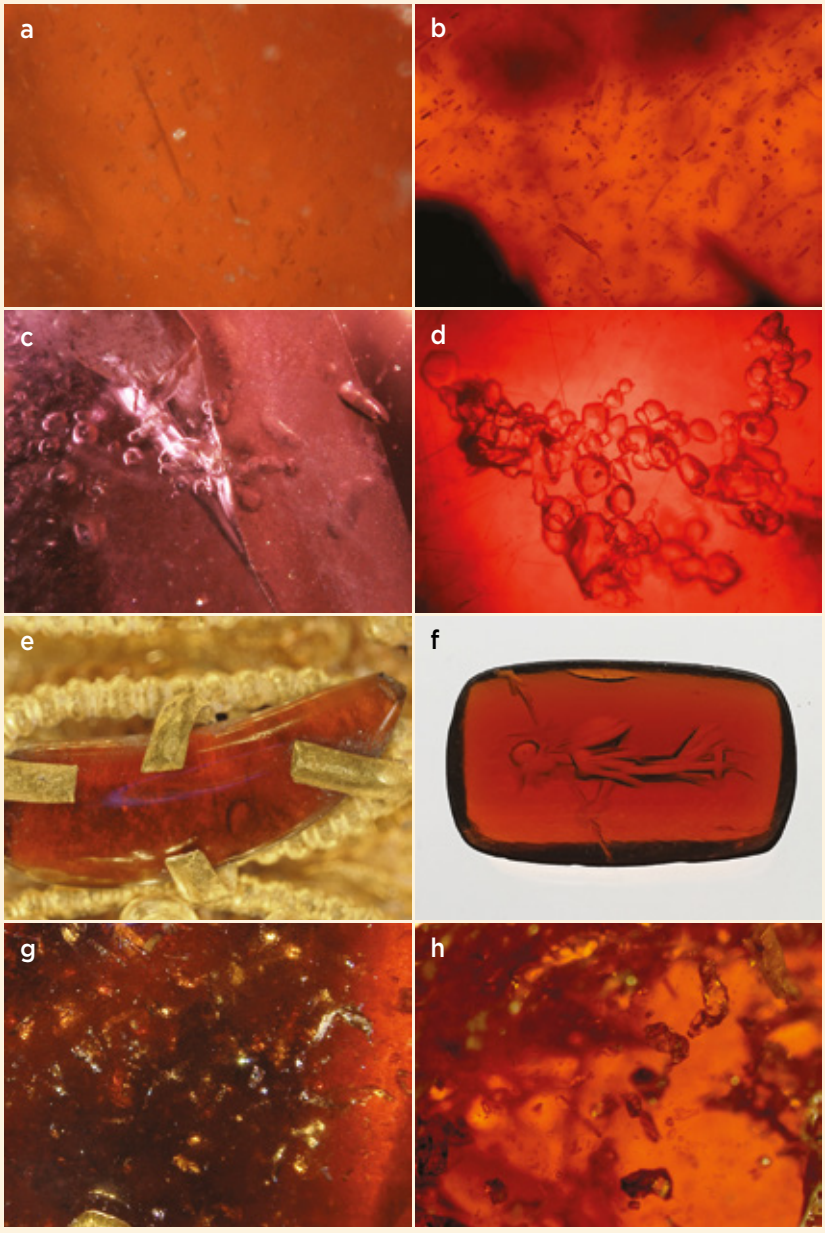

Figure 20: Inclusions in other garnet types of the crown are shown with comparison samples. (Note that inclusion minerals were identified by Raman spectroscopy only in the comparison samples.) Equant to needle-shaped mineral inclusions ('dashes and dots') are present in both (**a**) pyrope-almandine A29 (image width 0.9 mm) and (**b**) a comparison Ca-rich pyrope-almandine from Anuradhapura, Sri Lanka (image width 1.3 mm). Agglomerations of roundish apatite are present in (**c**) pyrope-almandine A29 (image width 2 mm) and (**d**) a comparison Hellenistic engraved Ca-poor, almandine-rich pyrope (Staatliche Antikensammlung München, inv. no. NI 15.046-473; image width 1.3 mm). (**e**) Pyrope A37, most likely an antique reused stone, does not show any visible inclusions (image width 1.2 cm). (**f**) Analogously, this cluster D pyrope (a Roman engraved gem from Staatliche Antikensammlung München, inv. no. NI 15.046-069; 1.3 cm long) appears inclusion-free. (**g**) Grossular E16 shows numerous elongated, rounded inclusions (image width 8.9 mm). (**h**) Large apatite inclusions with a similar appearance are seen in a grossular (hessonite) from Kamburupitiya, Sri Lanka (image width 5.1 mm). Photomicrographs a, c, e and g © KHM-Museumsverband (Herbert Reitschuler); reproduced with permission. Photomicrographs b, d, f and h by H. A. Gilg.

obtained from stone A3 (Figure 12b), whereas sample A25 (Figure 12a) yielded clearly different spectral characteristics.

Emission lines in the PL spectrum of A25 were significantly broader, and the rather complex fine structure of the emission was not present (Figure 21). Such 'blurred' PL patterns have, to the best of our knowledge, only been obtained thus far from heat-treated natural gem spinel (Smith 2012; Peretti *et al.* 2015; Widmer *et al.* 2015), or from high-temperature synthetic (i.e. melt-grown) spinel that typically has a somewhat non-stoichiometric chemical composition (Mohler & White 1995; Dereń *et al.* 1996; Peretti *et al.* 2015). As the setting of spinel A25 in the crown seems to be original, and since gem-quality synthetic red spinel was available only in recent times (e.g. Muhlmeister *et al.* 1993), it appears impossible that A25 could be a synthetic spinel. Therefore, the broadened PL spectrum points to a heated natural stone.

Similarly, the Raman band pattern of A25 was broadened, with clear asymmetry of the main 407–408 cm^{-1} E_g band towards the low-energy side (Figure 22). Such Raman spectra are typical for heated natural gem spinel (Van Minh & Yang 2004; Slotznick & Shim 2008; Widmer *et al.* 2015). This is supported by the presence of an additional band near 724 cm^{-1} in the Raman spectrum, which is not, or with only very low intensity, present in the spectra of non-heat-treated natural Mg-Al spinel. This band has been assigned to structural disorder caused by heat-induced cation inversion, which may cause 'normal' spinel to shift towards 'inverse' spinel[1] (Cynn *et al.* 1992; Slotznick & Shim 2008; Ma *et al.* 2022). Widmer *et al.* (2015) found that heating of spinel for 72 hours to 700°C, followed by slow cooling, did not result in any measurable Raman spectral changes. Correspondingly, Liu *et al.* (2022) did not find significant spectral changes after heating for two hours up to 750°C; they obtained a broadened emission spectrum corresponding to that of spinel A25 only after heating at 1000°C. Spectra obtained from our own heat treatment experiments (Figures 21 and 22) confirm these results: spinel A25 must have experienced heating up to well above 700°C, perhaps close to 1000°C.

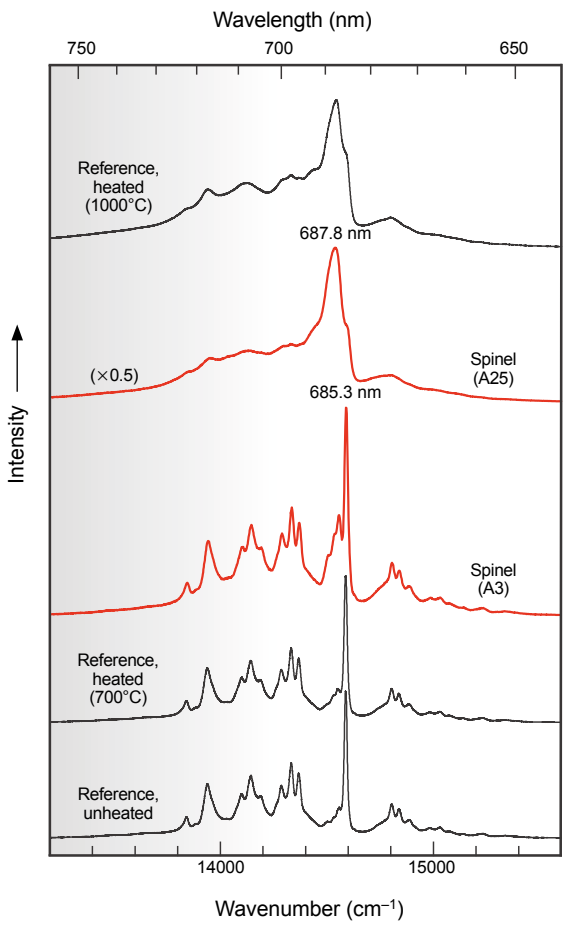

Figure 21: Laser-induced PL spectra (457 nm excitation) are shown for 'normal' spinel A3 and significantly 'inverse' spinel A25, in comparison with reference spectra (473 nm excitation) for a gem spinel from Ratnapura, Sri Lanka (unheated and heated to 700°C and 1000°C). For spinel A25, note the low degree of emission fine-structure, consistent with the reference spinel that was heated to 1000°C. The spectral range not visible to the human eye is shaded grey. Spectra are offset vertically for clarity.

It therefore appears that red stone A25 is a natural

[1] The term 'normal' refers to a so-called normal cation occupation in the spinel structure (that is, four-coordinated divalent cations and six-coordinated trivalent cations). Natural Mg-Al spinel typically has (close to) 'normal' cation occupation, whereas other members of the spinel supergroup (Bosi *et al.* 2019), such as magnetite, are 'inverse' (that is, divalent cations occupy a six-coordinated site and half of the trivalent cations occupy a four-coordinated site). Heating of predominantly 'normal' Mg-Al spinel to above 700–800°C, especially (but not necessarily) when followed by more-or-less rapid cooling, causes irreversible structural perturbation by significantly increasing the degree of cation inversion to well above 20% (Van Minh & Yang 2004; Slotznick & Shim 2008; Ma *et al.* 2022), according to the following:

$^{IV}Mg^{VI}Al_2O_4 \rightarrow {}^{IV}(Mg_{1-i}Al_i)^{IV}(Al_{2-i}Mg_i)O_4$

where i = a parameter describing the degree of proportionately inverse cation occupation (Wood *et al.* 1986).

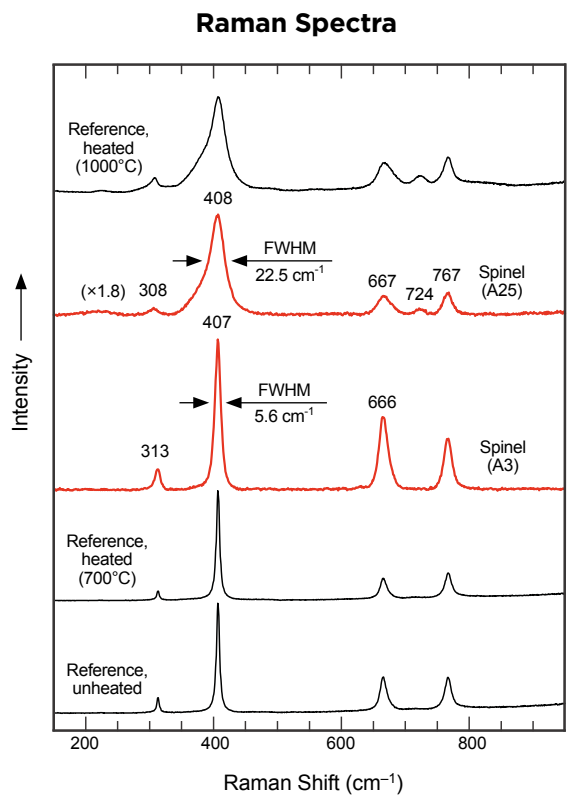

Figure 22: Raman spectra (457 nm excitation) are shown for the same samples as in Figure 21. For spinel A25, note the asymmetry and broad width of the main Raman band; analogous spectral changes of the reference spinel were achieved only after heating to well above 700°C. Quoted FWHM values are corrected for experimental band broadening. Spectra are offset vertically for clarity.

spinel that was heated before being set into the Imperial Crown. At the time the Imperial Crown was manufactured, the most common gem enhancements were dyeing, oiling, coating and foiling (Nassau 1984; Karampelas *et al*. 2020), but there have been a number of reports of very early heating of gems. For example, heating of microcrystalline silica was done as early as the Pre-Pottery Neolithic period to make it easier to shape beads and to enhance the colour of carnelian (Coşkunsu 2008; Groman-Yaroslavski & Bar-Yosef Mayer 2015)—techniques brought to perfection by the Indus Valley civilisation during the Bronze Age (Roux 2000; Possehl 2002). Heat treatments to improve colour and transparency of hard red, blue and yellow gemstones (termed *yaqut* in Arabic) have been mentioned frequently in Arabic mineralogical texts since the ninth century CE (e.g. Ruska 1912; Said 1989; Huda 1998; Troupeau 1998; Content 2016). It has generally been assumed that *yaqut* refers to gem corundum (ruby and sapphire), but this term might have also included spinel, as red *yaqut* weighing more than 200 ct have been described (Qaddumi 1996; Content 2016). Consequently, it needs to be taken into consideration that, as early as more than 1,000 years ago, spinel A25 could have been subjected to intentional heating for colour or clarity enhancement.

The possibility that the stone was accidentally exposed to fire before being set in the crown also needs to be considered. It has been known for a long time that accidental heating can affect gem properties. Köhler (1877) reported an early example: after the house of a miner burned down in 1757, 50 kg of previously wine-yellow Schneckenstein topaz turned colourless. Heating of spinel A25 in the course of experimental, traditional or religious practices (such as to prove imperishable durability or the like) could be another possibility. Two drill holes, one at the upper end and one on the bottom side of A25, lead to the presumption that this spinel had already been mounted in another object before its placement in the Imperial Crown. A link between this former usage and the ascertained heating of the stone is also worth considering. Overall, spinel A25 is most remarkable because, to our knowledge, it represents one of the earliest uses of this mineral as a gemstone, as well as the earliest known heat-treatment of this gem material. Pink spinels first appeared in European and Asian jewellery in the thirteenth century (Content 2016; Bruni *et al*. 2021; Ogden 2021), slowly replacing dark garnets, but they became more common in the fourteenth century (e.g. Hyršl & Neumanova 1999; Schmetzer & Gilg 2020). This largest red gemstone in the crown was, therefore, a unique new gem material at that time with respect to transparency and size, and might have initiated the myth of the 'Orphan Stone'.

CONCLUSION

One general limiting factor in analysing gemstones in archaeological and art-historical specimens is that, in many cases, objects cannot be taken to a laboratory; instead, analytical devices need to be brought to the objects. This includes immovable items such as sculptures and wall tessellations, as well as objects with enormous historical and/or monetary value, or those where a critical state of preservation does not allow transportation.

Many successful spectroscopic studies have been conducted on-site using small, portable systems. Most of these units, however, have the drawback that only limited (and in some cases fixed, pre-set) spectral ranges can be detected. In our case, it was most beneficial to have

a research-grade spectrometer available that allowed us to analyse the full spectral range of interest (that is, from the blue to NIR region), because both laser-induced PL (cf. Tsai & D'Haenens-Johansson 2021) and Raman spectra could be obtained and interpreted. Apart from the information gained, the use of PL proved advantageous simply because electronic emissions, compared to Raman-scattered light, are often several orders of magnitude higher in intensity and, hence, much more easily detected. Another advantage of the spectrometer used in this study, compared to small gem-testing Raman devices, was its reasonable spectral resolution. The latter helps resolve closely adjacent spectroscopic signals and evaluate band shapes.

All 172 gemstones in the Imperial Crown of the Holy Roman Empire were successfully identified (again, see Figure 8). Apart from some unexpected results—such as for stones A3 (pink spinel) and K26 (pale amethyst underlain by a reddish substance) that were initially assumed to be corundum—the previous assignments of most large stones were confirmed. Most of the small gems in the crown have, to the best of our knowledge, never been appropriately studied or identified before.

Beyond the identification of gem minerals in the crown, further interpretation—such as the comprehensive characterisation of the glass gems (chemical composition, degree of deterioration and possible origin)—remains speculative and requires additional analytical work. Moreover, chemical analysis of the enamel, pearls and selected gems in the crown will be the focus of our forthcoming second measurement campaign, and we plan to publish the results in a future issue of *The Journal*. These studies are part of an ongoing project that aims to capture and analyse as many details as possible concerning the Imperial Crown's materials, manufacturing techniques and history, with the objective of providing a profound basis for further research and interpretations pertaining to this crown.

REFERENCES

Antušková, V., Šefců, R., Šulcová, P., Dohnalová, Ž., Luxová, J., Bajeux Kmoníčková, M., Turková, I. & Kotrlý, M. 2022. Spectroscopic characterisation of Naples yellow variations in paintings from the turn of the 20th century. *Journal of Raman Spectroscopy*, **22**, article 6470, https://doi.org/10.1002/jrs.6470.

Bell, I.M., Clark, R.J.H. & Gibbs, P.J. 1997. Raman spectroscopic library of natural and synthetic pigments (pre- ≈ 1850 AD). *Spectrochimica Acta Part A: Molecular and Biomolecular Spectroscopy*, **53**(12), 2159–2179, https://doi.org/10.1016/s1386-1425(97)00140-6.

Beyssac, O. & Lazzeri, M. 2012. Application of Raman spectroscopy to the study of graphitic carbons in the earth sciences. *In*: Dubessy, J., Caumon, M.-C. & Rull, F. (eds) *Raman Spectroscopy Applied to Earth Sciences and Cultural Heritage*. European Mineralogical Union and the Mineralogical Society of Great Britain & Ireland, Twickenham, 415–454, https://doi.org/10.1180/EMU-notes.12.12.

Bosi, F., Biagioni, C. & Pasero, M. 2019. Nomenclature and classification of the spinel supergroup. *European Journal of Mineralogy*, **31**(1), 183–192, https://doi.org/10.1127/ejm/2019/0031-2788.

Brik, M.G., Papan, J., Jovanović, D.J. & Dramićanin, M.D. 2016. Luminescence of Cr^{3+} ions in $ZnA1_2O_4$ and $MgA1_2O_4$ spinels: Correlation between experimental spectroscopic studies and crystal field calculations. *Journal of Luminescence*, **177**, 145–151, https://doi.org/10.1016/j.jlumin.2016.04.043.

Bruni, Y., Hatert, F., George, P., Cambier, H. & Strivay, D. 2021. A gemmological study of the reliquary crown of Namur, Belgium. *European Journal of Mineralogy*, **33**(2), 221–232, https://doi.org/10.5194/ejm-33-221-2021.

Buettner, B. 2022. *The Mineral and the Visual: Precious Stones in Medieval Secular Culture*. Pennsylvania State University Press, University Park, Pennsylvania, USA, 272 pp.

Bugoi, R., Oanţă-Marghitu, R. & Calligaro, T. 2016. IBA investigations of loose garnets from Pietroasa, Apahida and Cluj-Someşeni treasures (5th century AD). *Nuclear Instruments and Methods in Physics Research Section B: Beam Interactions with Materials and Atoms*, **371**, 401–406, https://doi.org/10.1016/j.nimb.2015.09.038.

Calligaro, T., Colinart, S., Poirot, J.-P. & Sudres, C. 2002. Combined external-beam PIXE and μ-Raman characterisation of garnets used in Merovingian jewellery. *Nuclear Instruments and Methods in Physics Research Section B: Beam Interactions with Materials and Atoms*, **189**(1–4), 320–327, https://doi.org/10.1016/s0168-583x(01)01078-3.

Carter, A.K., Dussubieux, L., Stark, M.T. & Gilg, H.A. 2021. Angkor Borei and protohistoric trade networks: A view from the glass and stone bead assemblage. *Asian Perspectives*, **60**(1), 32–70, https://doi.org/10.1353/asi.2020.0036.

Colomban, P. 2003. Polymerization degree and Raman identification of ancient glasses used for jewelry, ceramic enamels and mosaics. *Journal of Non-Crystalline Solids*, **323**(1–3), 180–187, https://doi.org/10.1016/s0022-3093(03)00303-x.

Colomban, P., Etcheverry, M.-P., Asquier, M., Bounichou, M. & Tournié, A. 2006. Raman identification of ancient stained glasses and their degree of deterioration. *Journal of Raman Spectroscopy*, **37**(5), 614–626, https://doi.org/10.1002/jrs.1495.

Content, D.J. 2016. *Ruby, Sapphire & Spinel: An Archaeological, Textual and Cultural Study*. Brepols Publishers, Turnhout, Belgium, 452 pp.

Coşkunsu, G. 2008. Hole-making tools of Mezraa Teleilat with special attention to micro-borers and cylindrical polished drills and bead production. *Neo-Lithics*, **1**(8), 25–36, https://www.exoriente.org/repository/NEO-LITHICS/NEO-LITHICS_2008_1.pdf.

Cynn, H., Sharma, S.K., Cooney, T.F. & Nicol, M. 1992. High-temperature Raman investigation of order-disorder behavior in the $MgA1_2O_4$ spinel. *Physical Review B*, **45**(1), 500–502, https://doi.org/10.1103/PhysRevB.45.500.

Decker-Hauff, H. 1955. Die "Reichskrone" angefertigt für Kaiser Otto I. *In*: Schramm, P.E. (ed) *Herrschaftszeichen und Statussymbolik. Beiträge zu ihrer Geschichte vom dritten bis zum sechzehnten Jahrhundert. Monumenta Germaniae Historica.* Anton Hierseman Verlag, Stuttgart, Germany, **13**(II), 560–637.

Dereń, P.J., Malinowski, M. & Stręk, W. 1996. Site selection spectroscopy of Cr^{3+} in $MgA1_2O_4$ green spinel. *Journal of Luminescence*, **68**(2–4), 91–103, https://doi.org/10.1016/0022-2313(96)00020-8.

Etchepare, J., Merian, M. & Smetankine, L. 1974. Vibrational normal modes of SiO_2. I. α and β quartz. *Journal of Chemical Physics*, **60**(5), 1873–1876, https://doi.org/10.1063/1.1681287.

Fillitz, H. 1953. Studien zur römischen Reichskrone. *Jahrbuch der Kunsthistorischen Sammlungen in Wien*, **50**(14), 23–52.

Fillitz, H. 1956. Die Edelsteinordnung auf der Reichskrone und ihre Beziehung zur Spätantike. *Österreichische Zeitschrift für Kunst und Denkmalpflege*, **10**, 38–45.

Gartzke, E. 2004. *Methoden zur materialkundlichen Untersuchung antiker Schmuckstücke*. Master's thesis, University of Würzburg, Germany, 196 pp.

Gilg, H.A. & Gast, N. 2012. Naturwissenschaftliche Untersuchungen an Granatgemmen der Sammlung James Loeb. *In*: Weiss, C. & Knauss, F.S. (eds) *Die Gemmen der Sammlung James Loeb*. Kunstverlag Josef Fink, Lindenberg im Allgäu, Germany, 48–57, 62–63.

Gilg, H.A. & Gast, N. 2016. Determination of titanium content in pyrope by Raman spectroscopy. *Journal of Raman Spectroscopy*, **47**(4), 486–491, https://doi.org/10.1002/jrs.4838.

Gilg, H.A. & Hyršl, J. 2014. Garnet deposits in Europe. In: Toussaint, J. (ed) *Rouges et Noirs: Rubis, Grenat, Onyx, Obsidienne et Autres Minéraux Rouges et Noirs dans l'Art et l'Archéologie*. Société Archéologique de Namur, Namur, France, 144–173.

Gilg, H.A., Gast, N. & Calligaro, T. 2010. Vom Karfunkelstein. *In*: Wamser, L. (ed) *Karfunkelstein und Seide: neue Schätze aus Bayerns Frühzeit*. F. Pustet, Regensburg, Germany, 87–100.

Gilg, H.A., Schmetzer, K. & Schüssler, U. 2018. An Early Byzantine engraved almandine from the Garibpet deposit, Telangana State, India: Evidence for garnet trade along the ancient Maritime Silk Road. *Gems & Gemology*, **54**(2), 149–165, https://doi.org/10.5741/gems.54.2.149.

Gilg, H.A., Schüssler, U., Krause, J. & Schulz, B. 2019. The use of phosphate inclusions in origin determination of ancient and medieval red garnets. *36th International Gemmological Conference*, Nantes, France, 27–31 August, 41–43.

Greiff, S. 2010. Zur Herkunft der roten Granate an Schmuckobjekten des Erfurter Schatzfundes. *In*: Ostritz, S. (ed) *Die mittelalterliche jüdische Kultur in Erfurt. Band 2. Der Schatzfund: Analysen – Herstellungstechniken – Rekonstruktionen*. Thüringisches Landesamt für Denkmalpflege und Archäologie, Weimar, Germany, 482–487.

Groman-Yaroslavski, I. & Bar-Yosef Mayer, D.E. 2015. Lapidary technology revealed by functional analysis of carnelian beads from the early Neolithic site of Nahal Hemar Cave, southern Levant. *Journal of Archaeological Science*, **58**, 77–88, https://doi.org/10.1016/j.jas.2015.03.030.

Hagemann, H., Lucken, A., Bill, H., Gysler-Sanz, J. & Stalder, H.A. 1990. Polarized Raman spectra of beryl and bazzite. *Physics and Chemistry of Minerals*, **17**(5), 395–401, https://doi.org/10.1007/bf00212207.

Hofmeister, A.M. & Chopelas, A. 1991. Vibrational spectroscopy of end-member silicate garnets. *Physics and Chemistry of Minerals*, **17**(6), 503–526, https://doi.org/10.1007/bf00202230.

Huda, S.N.A. (transl.) 1998. *Arab Roots of Gemology: Ahmad ibn Yusuf Al Tifaschi's 'Best Thoughts on the Best of Stones'*. Scarecrow Press Inc., Lanham, Maryland, USA and London, 271 pp.

Huong, L.T.-T., Häger, T. & Hofmeister, W. 2010. Confocal micro-Raman spectroscopy: A powerful tool to identify natural and synthetic emeralds. *Gems & Gemology*, **46**(1), 36–41, https://doi.org/10.5741/gems.46.1.36.

Hyršl, J. & Neumanova, P. 1999. Eine neue gemmologische Untersuchung der Sankt Wenzelskrone in Prag. *Gemmologie: Zeitschrift der Deutschen Gemmologischen Gesellschaft*, **48**(1), 29–36.

Karampelas, S., Kiefert, L., Bersani, D. & Vandenabeele, P. 2020. Gem treatments, synthetics and imitations. *In: Gems and Gemmology*. Springer, Cham, Switzerland, 67–90, https://doi.org/10.1007/978-3-030-35449-7_4.

Kisliuk, P. & Moore, C.A. 1967. Radiation from the $^4T_2$ state of Cr^{3+} in ruby and emerald. *Physical Review*, **160**(2), 307–312, https://doi.org/10.1103/PhysRev.160.307.

Klaar, K.-E. 1986. Sicherung und Pflege der Reichskleinodien in Nürnberg. *In*: Schuhmann, G. (ed) *Nürnberg – Kaiser und Reich*. Ausstellungskataloge der staatlichen Archive Bayerns, Neustadt an der Aisch, Germany, **20**, 71–79.

Klee, W.E. 1970. The vibrational spectra of the phosphate ions in fluorapatite. *Zeitschrift für Kristallographie*, **131**(1–6), 95–102, https://doi.org/10.1524/zkri.1970.131.1-6.95.

Köhler, E. 1877. Ein Beitrag zur Geschichte des Topasfels Schneckenstein. *In*: Usbeck, O. (ed) *Mittheilungen des Vogtländischen Vereins für allgemeine und spezielle Naturkunde in Reichenbach i.V.*, Vol. 3, 29–38.

Kolesov, B.A. & Geiger, C.A. 1998. Raman spectra of silicate garnets. *Physics and Chemistry of Minerals*, **25**(2), 142–151, https://doi.org/10.1007/s002690050097.

Kos, S., Dolenec, M., Lux, J. & Dolenec, S. 2020. Raman microspectroscopy of garnets from S-fibulae from the archaeological site Lajh (Slovenia). *Minerals*, **10**(4), https://doi.org/10.3390/min10040325.

Kugler, G.J. 1986. *Die Reichskrone*. Herold-Verlag, Vienna, Austria, 158 pp.

Leute, M.A. 2000. *Mineralogische Charakterisierung der Radentheiner und Zillertaler Schmuckgranate, Österreich*. Unpublished Diploma thesis, University of Vienna, Austria, 129 pp.

Liu, Y., Qi, L., Schwarz, D. & Zhou, Z. 2022. Color mechanism and spectroscopic thermal variation of pink spinel reportedly from Kuh-i-Lal, Tajikistan. *Gems & Gemology*, **58**(3), 338–353, https://doi.org/10.5741/gems.58.3.338.

Ma, Y., Bao, X., Sui, Z., Zhao, X. & Liu, X. 2022. Quantifying Mg–Al cation distribution in $MgA1_2O_4$-spinel using Raman spectroscopy: An experimental calibration. *Solid Earth Sciences*, **7**(1), 60–71, https://doi.org/10.1016/j.sesci.2021.09.002.

Mathavan, V., Kalubandara, S.T. & Fernando, G.W.A.R. 2000. Occurrences of two new types of gem deposits in the Okkampitiya gem field, Sri Lanka. *Journal of Gemmology*, **27**(2), 65–72, https://doi.org/10.15506/JoG.2000.27.2.65.

Mentzel-Reuters, A. 2004. Die goldene Krone: Entwicklungslinien mittelalterlicher Herrschaftssymbolik. *Deutsches Archiv für Erforschung des Mittelalters*, **60**, 135–182, https://www.mgh-bibliothek.de/dokumente/a/a123901.pdf.

Mikenda, W. & Preisinger, A. 1981. N-lines in the luminescence spectra of Cr^{3+}-doped spinels: (II) Origins of N-lines. *Journal of Luminescence*, **26**(1–2), 67–83, https://doi.org/10.1016/0022-2313(81)90170-8.

Mohler, R.L. & White, W.B. 1995. Influence of structural order on the luminescence of oxide spinels: Cr^{3+}-activated spinels. *Journal of the Electrochemical Society*, **142**(11), 3923–3927, https://doi.org/10.1149/1.2048435.

Muhlmeister, S., Koivula, J.I., Kammerling, R.C., Smith, C.P., Fritsch, E. & Shigley, J.E. 1993. Flux-grown synthetic red and blue spinels from Russia. *Gems & Gemology*, **29**(2), 81–98, https://doi.org/10.5741/gems.29.2.81.

Nassau, K. 1984. The early history of gemstone treatments. *Gems & Gemology*, **20**(1), 22–33, https://doi.org/10.5741/gems.20.1.22.

Nelson, D.F. & Sturge, M.D. 1965. Relation between absorption and emission in the region of the *R* lines of ruby. *Physical Review*, **137**(4A), A1117–A1130, https://doi.org/10.1103/PhysRev.137.A1117.

Neuville, D.R. 2006. Viscosity, structure and mixing in (Ca, Na) silicate melts. *Chemical Geology*, **229**(1–3), 28–41, https://doi.org/10.1016/j.chemgeo.2006.01.008.

Ogden, J.M. 2021. Gem knowledge in the thirteenth century: The St Albans jewels. *Journal of Gemmology*, **37**(8), 816–834, https://doi.org/10.15506/JoG.2021.37.8.816.

Ollier, N., Fuchs, Y., Cavani, O., Horn, A.H. & Rossano, S. 2015. Influence of impurities on Cr^{3+} luminescence properties in Brazilian emerald and alexandrite. *European Journal of Mineralogy*, **27**(6), 783–792, https://doi.org/10.1127/ejm/2015/0027-2484.

Peretti, A., Tun, N.L. & Armbruster, T. 2015. Heat-treatment of spinels. *Contributions to Gemology*, No. 11, 269–278, https://www.gemresearch.ch/assets/documents/publication-articles/2015-05-spinel-heat-treatment-1.pdf.

Pinet, M. & Smith, D.C. 1994. La microspectrométrie Raman des grenats $X_3Y_2Z_3O_{12}$: II. La série alumineuse naturelle pyrope-almandine-spessartite. *Schweizerische Mineralogische und Petrographische Mitteilungen*, **74**(2), 161–179, https://doi.org/10.5169/seals-56339.

Porto, S.P.S. & Krishnan, R.S. 1967. Raman effect of corundum. *Journal of Chemical Physics*, **47**(3), 1009–1012, https://doi.org/10.1063/1.1711980.

Possehl, G.L. 2002. *The Indus Civilization: A Contemporary Perspective*. Rowman Altamira Press, Walnut Creek, California, USA, 276 pp.

Powell, R.C., DiBartolo, B., Birang, B. & Naiman, C.S. 1967. Fluorescence studies of energy transfer between single and pair Cr^{3+} systems in $A1_2O_3$. *Physical Review*, **155**(2), 296–308, https://doi.org/10.1103/PhysRev.155.296.

Qaddumi, G.H. (transl.) 1996. *Book of Gifts and Rarities (Kitāb al-Hadāyā wa al-Tuḥaf)*. Harvard University Press, Cambridge, Massachusetts, USA, 551 pp.

Quenstedt, F. 2022. *Der Waise: Transkulturelle Verflechtungen eines mittelalterlichen Kronjuwels*.

Logbuch Wissensgeschichte des SFB Episteme in Bewegung, Freie Universität Berlin, Germany, https://www.logbuch-wissensgeschichte.de/2390/der-waise, accessed 26 September 2022.

Rividi, N., van Zuilen, M., Philippot, P., Ménez, B., Godard, G. & Poidatz, E. 2010. Calibration of carbonate composition using micro-Raman analysis: Application to planetary surface exploration. *Astrobiology*, **10**(3), 293–309, https://doi.org/10.1089/ast.2009.0388.

Rösch, C., Hock, R., Schüssler, U., Yule, P. & Hannibal, A. 1997. Electron microprobe analysis and X-ray diffraction methods in archaeometry: Investigations on ancient beads from the Sultanate of Oman and from Sri Lanka. *European Journal of Mineralogy*, **9**(4), 763–783, https://doi.org/10.1127/ejm/9/4/0763.

Rothamel, U., Heber, J. & Grill, W. 1983. Vibronic sidebands in ruby. *Zeitschrift für Physik B Condensed Matter*, **50**(4), 297–304, https://doi.org/10.1007/bf01470041.

Roux, V. 2000. *Cornaline de l'Inde: Des Pratiques Techniques de Cambay aux Techno-systèmes de l'Indus*. Éditions de la Maison des Sciences de l'Homme, Paris, France, 558 pp., https://doi.org/10.4000/books.editionsmsh.8706.

Ruska, J. 1912. *Das Steinbuch des Aristoteles*. Carl Winter's Universitätsbuchhandlung, Heidelberg, Germany, vii + 208 pp., https://archive.org/details/dassteinbuchdesa00aris.

Said, H.M. (transl.) 1989. *Kitāb al-Jamāhir fī Ma'rifat al-Jawāhir (The Book Most Comprehensive in Knowledge on Precious Stones: Al-Beruni's Book on Mineralogy)*. Pakistan Hijra Council, Islamabad, Pakistan, xxix + 355 pp.

Schaller, H.M. 1997. Die Wiener Reichskrone – entstanden unter König Konrad III. *In*: Becker, H.-J. (ed) *Die Reichskleinodien. Herrschaftszeichen des Heiligen Römischen Reiches*. Schriften zur staufischen Geschichte und Kunst, Göppingen, Germany, **16**, 58–105.

Schmetzer, K. & Gilg, H.A. 2020. The late 14th-century royal crown of Blanche of Lancaster—History and gem materials. *Journal of Gemmology*, **37**(1), 26–64, https://doi.org/10.15506/JoG.2020.37.1.26.

Schmetzer, K., Gilg, H.A., Schüssler, U., Panjikar, J., Calligaro, T. & Périn, P. 2017. The linkage between garnets found in India at the Arikamedu archaeological site and their source at the Garibpet deposit. *Journal of Gemmology*, **35**(7), 598–627, https://doi.org/10.15506/JoG.2017.35.7.598.

Schmidt, P., Bellot-Gurlet, L., Leá, V. & Sciau, P. 2014. Moganite detection in silica rocks using Raman and infrared spectroscopy. *European Journal of Mineralogy*, **25**(5), 797–805, https://doi.org/10.1127/0935-1221/2013/0025-2274.

Schulze-Dörrlamm, M. 1991. *Die Kaiserkrone Konrads II. (1024 - 1039). Eine archäologische Untersuchung zu Alter und Herkunft der Reichskrone*. Thorbecke Verlag, Sigmaringen, Germany, 145 pp.

Schüssler, U., Rösch, C. & Hock, R. 2001. Beads from ancient Sri Lanka – First results of a systematic material analysis. *In*: Weisshaar, H.J., Roth, H. & Wijeyapala, W. (eds) *Ancient Ruhuna. Sri Lankan–German Archaeological Project in the Southern Province*, Vol. 1. Verlag Philipp von Zabern, Mainz am Rhein, Germany, 227–242.

Šefců, R., Chlumská, Š. & Hostašová, A. 2015. An investigation of the lead tin yellows type I and II and their use in Bohemian panel paintings from the Gothic period. *Heritage Science*, **3**(1), article 16, https://doi.org/10.1186/s40494-015-0045-2.

Slotznick, S.P. & Shim, S.H. 2008. In situ Raman spectroscopy measurements of $MgA1_2O_4$ spinel up to 1400 °C. *American Mineralogist*, **93**(2–3), 470–476, https://doi.org/10.2138/am.2008.2687.

Smith, C.P. 2012. Spinel and its treatments: A current status report. *InColor*, No. 19, 50–54, http://www.incolormagazine.com/books/pcpz/#p = 50.

Staats, R. 2006. *Die Reichskrone: Geschichte und Bedeutung eines europäischen Symbols*. Steve-Holger Ludwig, Kiel, Germany, 125 pp.

Then-Obłuska, J., Gilg, H.A., Schüssler, U. & Wagner, B. 2021. Western connections of northeast Africa: The garnet evidence from late antique Nubia, Sudan. *Archaeometry*, **63**(2), 227–246, https://doi.org/10.1111/arcm.12607.

Thoresen, L. & Schmetzer, K. 2013. Greek, Etruscan and Roman garnets in the antiquities collection of the J. Paul Getty Museum. *Journal of Gemmology*, **33**(7), 201–222, https://doi.org/10.15506/JoG.2013.33.7.201.

Troupeau, G. 1998. Le premier traité arabe de minéralogie: Le livre de Yūḥannā Ibn Māsawayh sur les pierres précieuses. *Annales Islamologiques*, **32**(6), 219–238, https://www.ifao.egnet.net/anisl/32/12.

Tsai, T.-H. & D'Haenens-Johansson, U.F.S. 2021. Rapid gemstone screening and identification using fluorescence spectroscopy. *Applied Optics*, **60**(12), 3412–3421, https://doi.org/10.1364/ao.419885.

Váczi, T. 2014. A new, simple approximation for the deconvolution of instrumental broadening in spectroscopic band profiles. *Applied Spectroscopy*, **68**(11), 1274–1278, https://doi.org/10.1366/13-07275.

Van Minh, N. & Yang, I.-S. 2004. A Raman study of cation-disorder transition temperature of natural $MgA1_2O_4$ spinel. *Vibrational Spectroscopy*, **35**(1–2), 93–96, https://doi.org/10.1016/j.vibspec.2003.12.013.

White, W.B. & DeAngelis, B.A. 1967. Interpretation of the vibrational spectra of spinels. *Spectrochimica Acta Part A: Molecular Spectroscopy,* **23**(4), 985–995, https://doi.org/10.1016/0584-8539(67)80023-0.

Whitney, D.L. & Evans, B.W. 2010. Abbreviations for names of rock-forming minerals. *American Mineralogist*, **95**(1), 185–187, https://doi.org/10.2138/am.2010.3371.

Widmer, R., Malsy, A.-K. & Armbruster, T. 2015. Effects of heat treatment on red gemstone spinel: Single-crystal X-ray, Raman, and photoluminescence study. *Physics and Chemistry of Minerals*, **42**(4), 251–260, https://doi.org/10.1007/s00269-014-0716-7.

Wolf, G.G. 1995. *Die Wiener Reichskrone*. Skira, Milan, Italy, 203 pp.

Wood, B.J., Kirkpatrick, R.J. & Montez, B. 1986. Order-disorder phenomena in $MgA1_2O_4$ spinel. *American Mineralogist*, **71**(7–8), 999–1006.

Zeug, M., Nasdala, L., Wanthanachaisaeng, B., Balmer, W.A., Corfu, F. & Wildner, M. 2018. Blue zircon from Ratanakiri, Cambodia. *Journal of Gemmology*, **36**(2), 112–132, https://doi.org/10.15506/JoG.2018.36.2.112.

Zeug, M., Nasdala, L., Chanmuang N, C. & Hauzenberger, C. 2022. Gem topaz from the Schneckenstein Crag, Saxony, Germany: Mineralogical characterization and luminescence. *Gems & Gemology*, **58**(1), 2–17, https://doi.org/10.5741/gems.58.1.2.

The Authors

Prof. Dr Lutz Nasdala*, Dr Chutimun Chanmuang N., Annalena Erlacher and Prof. Dr Gerald Giester
Institut für Mineralogie und Kristallographie, Universität Wien, Josef-Holaubek-Platz 2, 1090 Vienna, Austria
*Email: lutz.nasdala@univie.ac.at

Teresa Lamers, Dr Martina Griesser and Dr Franz Kirchweger
Kunsthistorisches Museum Vienna, Burgring 5, 1010 Vienna, Austria

Prof. Dr H. Albert Gilg
TUM School of Engineering and Design, Technische Universität München, Arcisstr. 21, 80333 Munich, Germany

Dr Miriam Böhmler
WITec Wissenschaftliche Instrumente und Technologie GmbH, Lise-Meitner-Straße 6, 89081 Ulm, Germany

Acknowledgements

Roman Schuckert and Erich Polacek (both from Universität Wien) are thanked for customising the Raman probe head and video camera to a tripod, including 3D printing of an adaptor plate. Dr Alexey Loparev (WITec GmbH, Ulm), Thomas Rosen and Wolfgang Zirbs (both from Universität Wien) provided software help. We are very much indebted to Helene Hanzer for her manifold help in the Imperial Treasury Vienna, Herbert Reitschuler for operating the digital microscope and taking the photographs that were used as a working basis and for presentation herein, Christian Mendez for many additional photographs and Sabine Stanek (all from Kunsthistorisches Museum Vienna) for assisting with the PL and Raman measurements. Sincere thanks to WITec Wissenschaftliche Instrumente und Technologie GmbH for loaning a spectrometer system, and to Kunsthistorisches Museum Vienna for the permission to use photographs and reproductions of documents herein. Author HAG is most grateful to the Staatliche Antikensammlung München and the Archäologische Staatssammlung (Munich, Germany) for the possibility to investigate garnets in their collections, and to Norbert Hommrichhausen (experimenta – The Science Center, Heilbronn, Germany) for help with Raman analysis and taking photographs of inclusions in reference garnets. We thank Prof. Dr Emmanuel Fritsch, Dr Stefanos Karampelas, Dr Radka Šefců and Dr Hao Wang for discussions and hints to literature. The constructive reviews of three anonymous experts and editorial help of Damon Strom are gratefully acknowledged. Author TL is recipient of a DOC fellowship of the Austrian Academy of Sciences at the Institute of Conservation and Restoration, University of Applied Arts Vienna. Research project 'Crown' is funded by Ernst von Siemens Kunststiftung and Rudolf August Oetker-Stiftung. Additional funding is supplied by the Federal Ministry for Arts, Culture, the Civil Service and Sport (BMKOES), Republic of Austria.